UNIVERSITY OF CALIFORNIA,
IRVINE

Propensity for Acute Supraspinatus Injury in Low-Speed Rear-End Automobile Collisions: A Biomechanical Perspective

THESIS

submitted in partial satisfaction of the requirements
for the degree of

MASTER OF SCIENCE

in Biomedical Engineering

by

Ross Craig Hunter

Thesis Committee:
Professor Thay Q. Lee, Chair
Professor David J. Reinkensmeyer
Professor Ranjan Gupta

2017

DEDICATION

I dedicate this thesis to my beloved wife, Miyu, without her help and great patience this research could not have been completed.

TABLE OF CONTENTS

LIST OF FIGURES

LIST OF TABLES

ACKNOWLEDGMENTS

I would like to express my deepest appreciation to my committee chair, Dr. Thay Q. Lee, for allowing me to be a part of your lab and patiently guiding me throughout my thesis research. This thesis would not have been possible without your support and insight.

I would like to thank Dr. Ranjan Gupta and Dr. David Reinkensmeyer for your advice and interest in this research.

I would like to thank my lab manager, Michelle McGarry, for all your assistance with the logistics of the experimental setup and use of laboratory equipment, as well as your assistance during experiments.

I would like to thank Dr. Yasuo Itami for your assistance with dissection and preparation of the specimens, as well as your assistance during experiments.

I would like to thank Dr. Stuart Green for all your words of wisdom during my research.

I would like to thank all members of Dr. Lee's lab for providing me with ideas and suggestions throughout my research.

I would like to thank Chris Furbish and his co-authors for sharing with me their images from their high-speed videos of drivers in low-speed rear-end collisions [SAE 2011-01-0275]. Your research was a critical starting point for my thesis. Thank you for giving me permission to use those images in my thesis.

I would like to thank MEA Forensic for allowing me to use their facility to measure volunteers in a driver seat. I also would like to thank my supervisor, Dr. John Gardiner, and our director of research, Dr. Gunter Siegmund, for allowing me to pursue a graduate degree during my employment and for providing me with suggestions during my research.

ABSTRACT OF THE THESIS

Propensity for Acute Supraspinatus Injury
in Low-Speed Rear-End Automobile Collisions:
A Biomechanical Perspective

By

Ross Craig Hunter

Master of Science in Biomedical Engineering

University of California, Irvine, 2017

Professor Thay Q. Lee, Chair

Automobile drivers with a diagnosed supraspinatus (SSP) tendon tear following a low-speed rear-end collision often allege the collision is responsible for causing their shoulder injury. The goal was to determine the propensity for acute tear of a healthy SSP tendon during a low-speed rear-end automobile collision. To accomplish this, first the scapula and humerus positions were measured in twenty-one volunteers while in a driver seat. Then these positions were averaged and simulated in a cadaver shoulder to explore three possible injury mechanisms for acute isolated SSP tendon tear: humeral head displacement, tendon impingement, and tendon tension.

With a balanced rotator cuff muscle load, the SSP muscle had the largest change in length for 5 of 8 directions of humeral head displacement; however, the muscle length in 7 of 8 humeral head displacements was less than the muscle length at maximum ROM and changes in SSP tendon length were minimal (0±1 mm) for all humeral head displacements. No acromial impingement of the distal SSP tendon occurred with any of the humeral head

displaced positions. Tensile testing of the humerus-SSP tendon complex resulted in a fracture of the humerus at 904 N.

These findings and review of literature suggest that a low-speed rear-end collision may not be an event that predisposes a healthy SSP tendon to tear. Tendon degeneration, non-uniform tendon loading, and pre-existing asymptomatic partial or full-thickness tendon tears may alter the risk of a SSP tendon tear or onset of pain in low-speed rear-end collisions.

INTRODUCTION

Frequency of Rotator Cuff Injuries and Rear-end Automobile Accidents

The shoulder provides the greatest range of motion of any joint in the body, but this range of motion comes at the cost of stability and injury [1, 2]. Each year there are approximately 4.5 million patients with symptoms of shoulder pain in the United States [3, 4]. The most common type of shoulder disability involves the rotator cuff [5-8]. The rotator cuff is comprised of four muscles (Figure 1) that originate on the scapula (shoulder blade) and its tendons attach to the head of the humerus (arm). A common rotator cuff injury is a tear of the supraspinatus (SSP) tendon at or near the insertion (Figure 2), for both acute traumatic tears as well as a chronic degenerative tears [9-16]. The prevalence of rotator cuff tears, particularly the SSP tendon, has been found to increase with age [16-19]; with estimates of 4% to 11% in patients under the age of 40 years and 20% to 50% in patients above the age of 60 years. Those who have been diagnosed with a rotator cuff tendon tear after a low-speed rear-end automobile accident might allege that the collision is responsible for causing their shoulder injury. An internet search on "rotator cuff injury in rear-end collision" provides numerous legal services and web articles regarding causation and compensation for rotator cuff injury, which suggests that this injury is frequently disputed in the event of an automobile accident.

The economic cost of non-fatal injuries from motor vehicle accidents in the United States was estimated in 2010 to be $159 billion [20]. Included in these amounts are lost productivity, medical costs, legal and court costs, emergency service costs, insurance administration costs, travel delay, property damage, and workplace losses. In 2014, there were over 2.3 million people injured in automobile accidents, 1.5 million of whom were

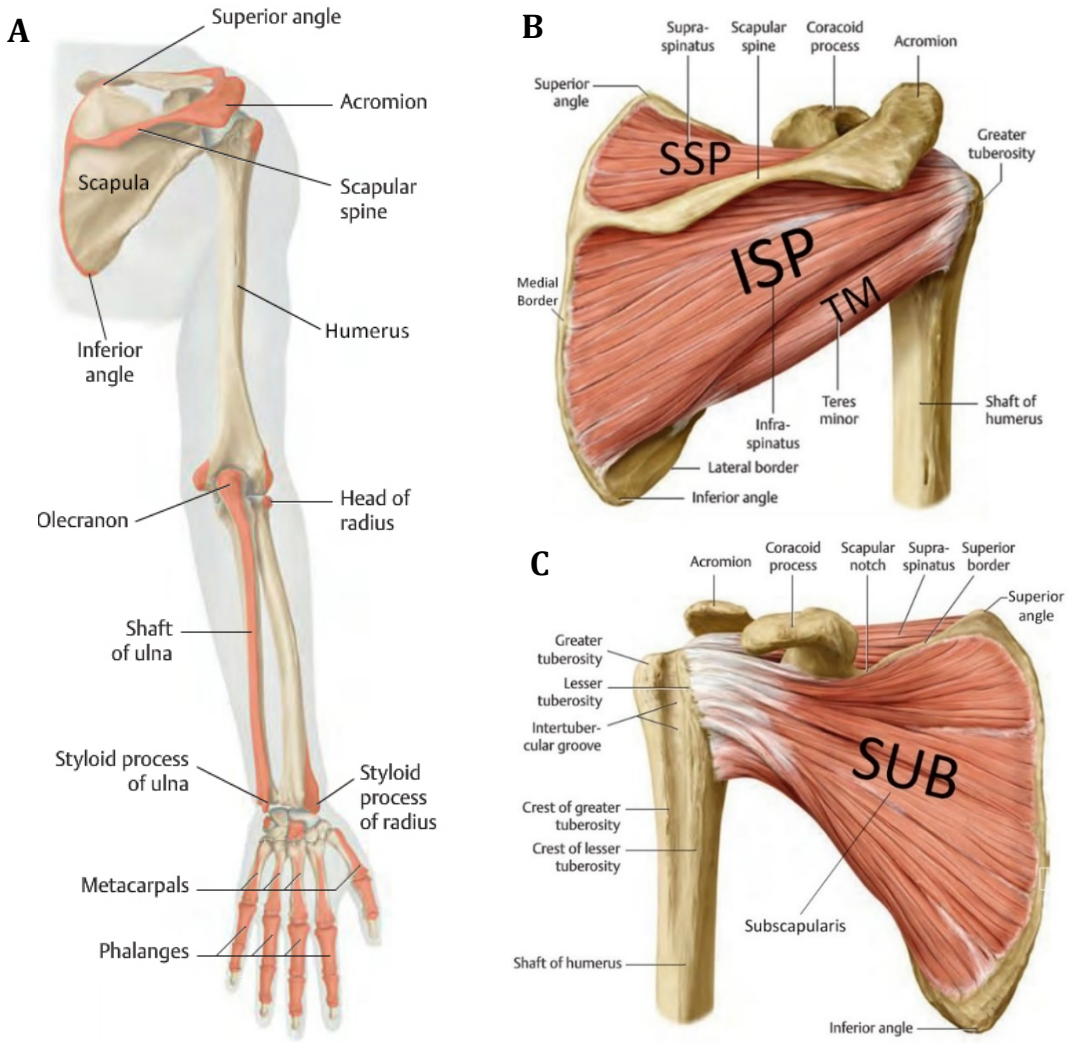

Figure 1: Illustration of the upper extremity bones and rotator cuff muscles of the shoulder (adapted from [21]). **(A)** Posterior view showing the scapula (shoulder blade) and the humerus (arm). **(B)** Posterior view of the rotator cuff muscles showing the supraspinatus (SSP), infraspinatus (ISP), and teres minor (TM). **(C)** Anterior view of the rotator cuff showing the large subscapularis (SUB) muscle.

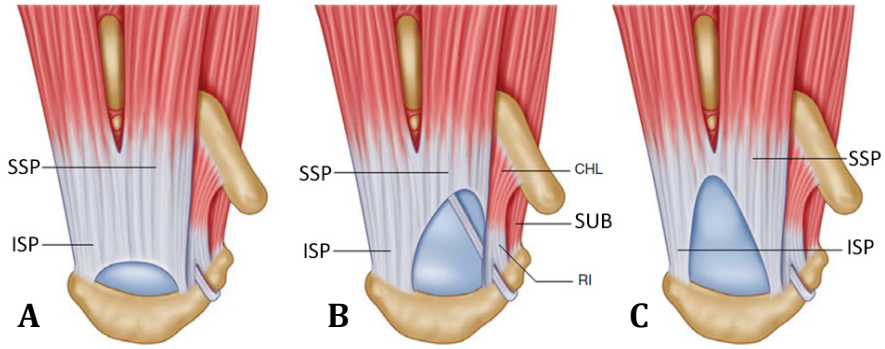

Figure 2: Superior view of full-thickness tears that span the width of the SSP and portion of the ISP tendons. Example tear shapes and size: **(a)** crescent, **(b)** reverse L-shaped, **(c)** U-shaped [22].

drivers [23]. Ninety-four percent of crashes were passenger cars (55.4%) or light trucks (38.7%). Roughly thirty percent of passenger car crashes and thirty percent of light truck crashes were rear-end collisions—resulting in a total of 591,000 injured occupants that year. Rear-end collisions have an injury rate of roughly 400 people for every 1000 crashes.

Driver Dynamics During a Low-Speed Rear-end Collision

Driver motion during low-speed rear-end collisions has been studied using human volunteers [24-41]. Upon impact, the front vehicle is pushed forward with respect to the ground and the driver moves rearward with respect to the vehicle interior (Figure 3A). The seatback initially rotates rearward due to the occupant inertia and then rebounds forward towards its original position, causing the driver to dynamically recline and then rebound forward towards the steering wheel (Figure 3A).

Majority of the loads to the shoulder during a collision occur indirectly through the arm from the steering wheel, whereas very little load is directly applied to the shoulder from the seatbelt [27, 42]. Several studies have shown that drivers who are unaware of the time of impact quickly lose their grip [27, 38, 39] and apply minimal loads to the steering wheel [27], which suggests that the hand/forearm muscle reaction time in a startle response may not be quick enough to maintain grip with steering wheel. However, drivers who were aware and braced for impact were able to maintain their grip during the collision [27]. The load applied to the steering wheel by a driver are first tensile as the driver moves rearward and then compressive as the driver rebounds forward [27]. Peak steering column tensile loads (Figure 3B) occur as the driver is in a reclined position with their elbows almost fully extended and peak steering column compressive loads occur as the driver approximately returns to their initial upright position. More examples of volunteer drivers in low-speed

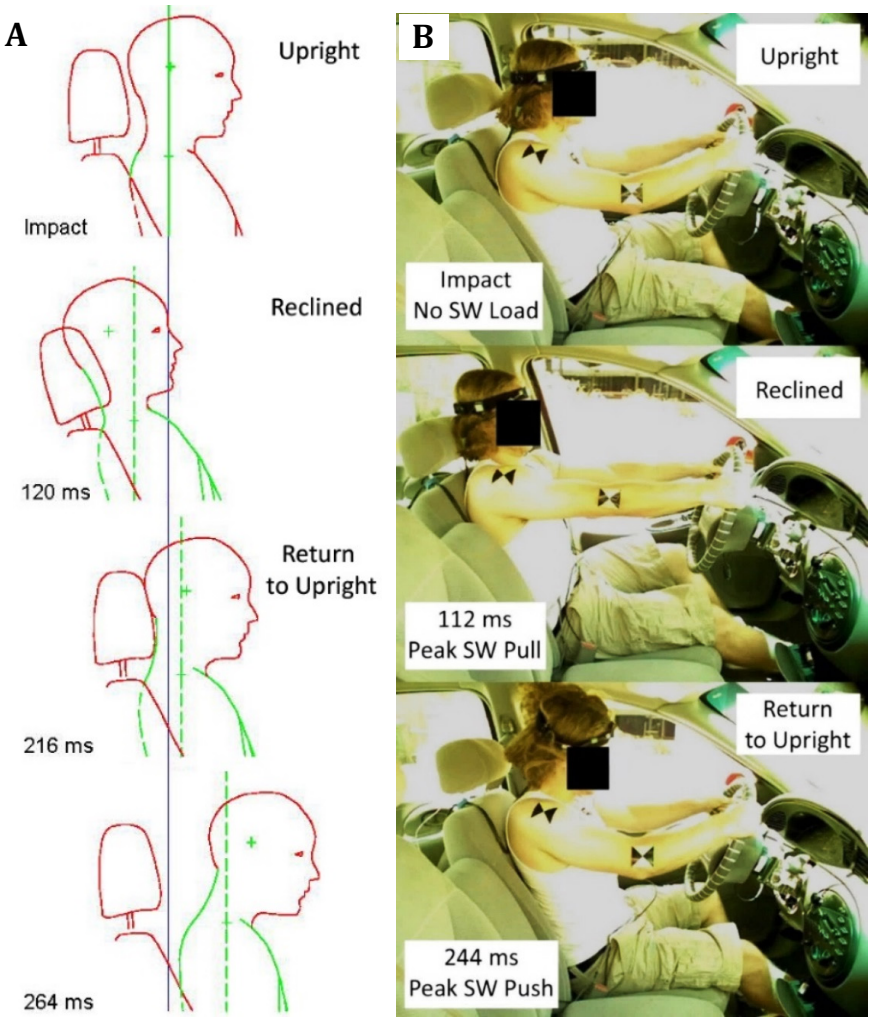

Figure 3: Driver motion during a low-speed rear-end impact. **(A)** Initial rearward motion followed by forward rebound (adapted from [36]). **(B)** Driver position at time of peak steering wheel (SW) loads [27].

rear-end collisions can be found in Appendix A. The direction of displacement of the humeral head relative to the glenoid fossa during tensile and compressive loads to the steering column is currently unknown. However, the magnitude of humeral head displacement is limited since low-speed rear-end collisions typically do not result in dislocations of the arm like that of some high-speed collisions.

Driver Rotator Cuff Muscle Activity

The rotator cuff muscles are active stabilizers of the glenohumeral joint that provide cavity compression to keep the humeral head in alignment with the glenoid fossa [1, 2, 43].

If the SSP muscle is active while the humerus is displaced away from the glenoid fossa, then the SSP will undergo eccentric muscle contraction, i.e. lengthening of the muscle as it actively contracts, thereby increasing the tension in the tendon.

Currently there are no available studies on the SSP muscle activity (muscle contraction) during a low-speed rear-end collision. Studies not related to automobile collisions suggest that braced drivers would have an activated SSP muscle before and during the collision. Increasing one's handgrip to 50% of max strength has been shown to increase SSP muscle electromyographic (EMG) activity [2, 44]; and similar dynamic movements, such as the upright chest press and row, also measured increased SSP muscle activity [45].

Impingement of Supraspinatus Tendon

Currently there are no available studies on the alignment of a driver's SSP tendon with internal bone structures during a rear-end collision. MRI of volunteers in a position somewhat similar to a driving position found that the distal SSP tendon during the Hawkin's impingement test posture (Figure 4A) was at an average distance of 4 ± 0.7 mm from the inferior surface of the anterior region of the acromion (Figure 4B) [46].

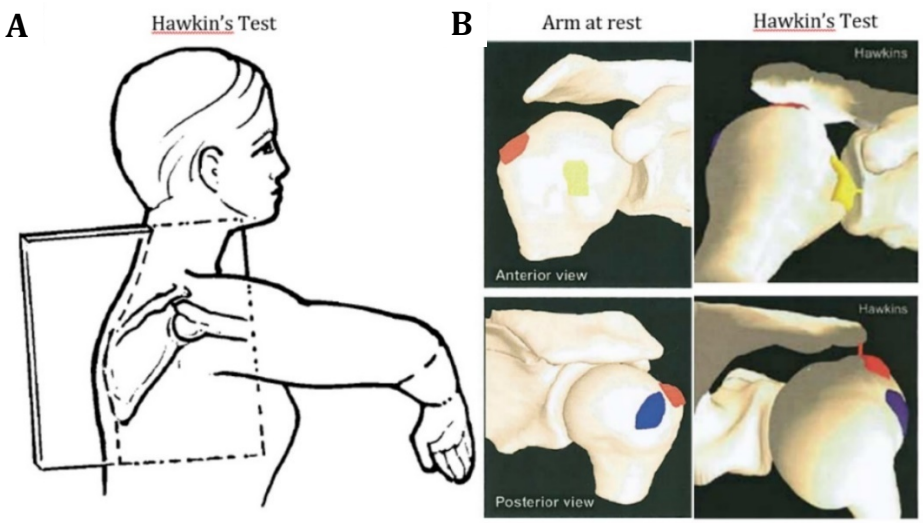

Figure 4: (A) Orientation of the scapula and humerus during a Hawkin's test posture [47]. **(B)** Location of the insertion of the SSP (red), the ISP (blue), and the SUB (yellow) relative to the acromion [46].

Scope of Research

The overall goal of this thesis was to determine the propensity for acute tear of a healthy SSP tendon during a low-speed rear-end automobile collision. To accomplish this, first the scapula and humerus positions were measured in twenty-one volunteers while in a driver seat. Then these positions were averaged and simulated in a cadaver shoulder to explore three possible injury mechanisms for acute isolated SSP tendon tear: humeral head displacement, tendon impingement, and tendon tension. The methods, results, and discussion of this research is divided into two experiments: Experiment A and Experiment B.

For Experiment A, human volunteers were statically measured in a driver seat while holding a steering wheel to determine overall external palpable geometry. Then the scapula and humerus of a cadaver was positioned in the average orientation of the volunteer measurements to approximate nonpalpable internal glenohumeral geometry. The hypothesis for Experiment A is that the scapula and humerus orientation will have a low standard deviation (≤10°), thereby allowing for a 47-year-old female cadaver to approximate glenohumeral alignment while positioned in the average orientation.

Experiment B was then performed on the same cadaver due to having a relatively young (≤50 years old [10]) and fully intact SSP tendon. Exploring the effects of tendon degeneration and pre-existing tears was beyond the scope of this master's thesis. Experiment B was divided into four main parts: P1) quantify the change in length of the SSP muscle and tendon due to humeral head displacement, P2) compare the SSP muscle length during humeral head displacement to the muscle length at the specimen's maximum range of motion (ROM), referred in short as tightness of the SSP muscle and, P3) assess potential

for distal SSP tendon impingement with the acromion during humeral head displacement, and P4) perform tensile testing of the SSP tendon to characterize the strength of the specimen's humerus-SSP tendon complex.

CHAPTER 1: Methods

Experiment A:

1.A.1 Scapula and Humerus Orientation of Volunteers in the Driving Position

Twenty-one human volunteers (11 female, 10 male) were measured while seated in a cut-away driver seat apparatus called a "buck" (Figure 5). The buck was cut from a passenger car (1999 Audi A4 four-door sedan). Approval from UC Irvine Institutional Review Board (IRB) to measure human volunteers in the driving position was obtained. Human volunteers, rather than cadavers, were needed due to a phenomenon known as the scapulohumeral rhythm [1, 48, 49]. As a person moves their arm, their muscles will involuntarily act in coordination to the arm movement to maintain glenohumeral joint alignment. The palpation technique in conjunction with a coordinate measuring machine called MicroScribe 3DLX (rather than imaging with surface skin markers) was chosen to measure the volunteers because the scapula's large subcutaneous motion during arm movements [48] would render the skin targets inaccurate. Palpation technique has been shown to be an accurate method of determining the orientation of a static scapula at various arm elevation angles [50, 51].

Recruitment was limited to volunteers between the ages of 40 to 60. Persons above the age of 60 are more likely to have a pre-existing degenerative rotator cuff tear [16-19, 52], which could result in an abnormal scapulohumeral rhythm [53-55]; and persons below the age of 40 are less likely to sustain a rotator cuff tear from indirect loading of the arm [10]. BMI was also limited to ≤30 to improve accuracy of palpation technique. All volunteers denied having shoulder pain and a history of shoulder injury or surgical treatment.

Table 1: Volunteer demographics for driver shoulder measurements.

n = 21	Age (years)	Height (cm)	Weight (kg)	BMI (kg/m^2)
Average ± SD	51 ± 7	167 ± 12	68 ± 15	24 ± 4
Range	40 - 60	145 - 191	45 - 90	19 - 30

Figure 5: Cut-away driver seat apparatus with soft green foam block attached to the seatback.

The height and weight of the volunteers (Table 1) were first measured using a Seca 213 stadiometer and an Ohaus ES200L weight scale respectively. Once seated, volunteers were asked to hold the steering wheel at the 10 and 2 o'clock position with their left and right hands respectively. A small gap between the seatback and the volunteer's upper back was created using a green foam block (3x4" Airtex Heavy Duty 100% Polyurethane) to provide space to palpate and measure the scapula (Figure 5). Volunteers were measured in two static seat configurations: the upright and reclined positions (Figure 6), as these are the two approx. positions in which peak steering wheel tensile and compressive loads occur.

The steering wheel tilt was fixed at the midpoint of the adjustable range, which was 19° from vertical. Driver height can correlate with seat position [56]; therefore, volunteers were asked to adjust the driver seat forward or backward until they felt a comfortable distance from the steering wheel. Volunteers were asked not to adjust the seatback angle (SBA), as seat recline preferences do not correlate with driver height [56]. Therefore,

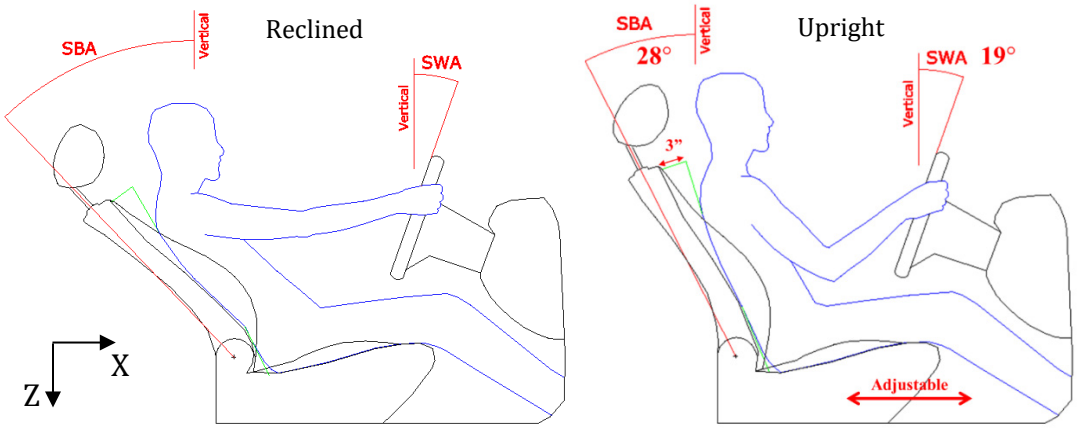

Figure 6: Illustration of a driver in the reclined position and upright position. Volunteers were allowed to adjust their seat forward or backward until they were a comfortable distance from the steering wheel. In the upright position, the seatback angle (SBA) was set to 28 degrees (equivalent to 22 degrees without a foam block). For the reclined position, the seatback was reclined until the volunteer's elbows were fully extended.

the seatback was set to an angle of 28 degrees from vertical for the upright position, which corresponded with a typical upright SBA of 22 degrees [56] had the green foam block not been attached to the seatback.

The first set of measurements was of the reference points on the driver seat and steering wheel to confirm that the seat did not move and to verify the seatback angle. A MicroScribe 3DLX (Immersion Corp, San Jose, California) was used to obtain XYZ coordinates of the driver seat reference points, which has an accuracy and repeatability of 0.3 and 0.2 mm respectively [57]. The global XYZ axes were based on the direction of the driver seat (Figure 6) where the X-axis is towards the front, Y-axis towards the right, and Z-axis downward in line with gravity. Three reference points on a fixed object independent of the buck were measured to make sure there was no shifting of the MicroScribe origin. The second set of MicroScribe measurements was of the volunteer's palpable bony landmarks. The palpable bony landmarks of the scapula and humerus include: the inferior angle, the root of the scapular spine, the posterolateral edge of the acromion, and the lateral and medial epicondyles (Figure 7A). To confirm repeatable grip position on the steering wheel,

forearm and hand reference measurements were also obtained, and included: the styloid processes of the ulna and radius and the metacarpophalangeal (MCP) joint of the third digit (Figure 7A). The coordinates of the bony landmarks were then used to calculate 3D Euler angle orientations for the scapula and humerus (Figure 7B).

The orientation of the scapula and humerus was determined by first establishing a local coordinate system for each bone (Figure 7B). The first vector established for the scapula was the Y-axis, which was from the root of the scapula spine to the posterolateral edge of the acromion. A cross-product of the y-axis and the vector from the root of the scapula spine to the inferior angle was used to obtain the scapula's X-axis. The scapula's Z-axis was obtained from the cross-product of the X- and Y-axes. A YX'Z'' Euler rotation sequence was used to calculate the scapula's orientation in terms of Y-axis posterior tilt (PT), X-axis upward rotation (UR), and Z-axis internal rotation (IR)/protraction. The first vector

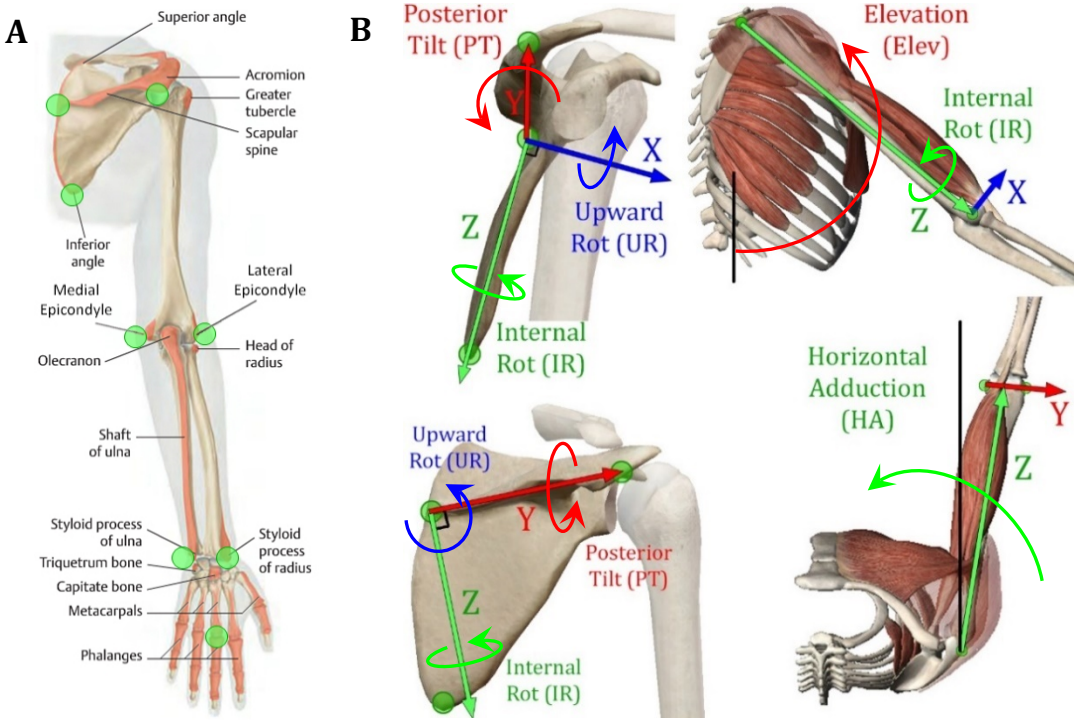

Figure 7: (A) Bony landmarks (green circles) used to determine scapula and humerus orientation in the driving position (adapted from [21]). **(B)** The 3D coordinates of the bony landmarks were used to calculate Euler angle orientation of the scapula and humerus (adapted from [58]).

established for the humerus was the Z-axis, which was from the posterolateral edge of the acromion to the midpoint between the lateral and medial epicondyles. Then the cross-product of the vector from the medial to the lateral epicondyles and the Z-axis was used to obtain the X-axis. The humerus Y-axis was obtained from the cross-product of the Z- and X-axes. A ZY'Z'' Euler rotation sequence was used to calculate the humerus horizontal adduction (HA), forward elevation (Elev), and internal rotation (IR)/axial rotation.

After completing the bony landmark measurements, the volunteer was asked to extend their arms beyond the steering wheel without lifting themselves off of the seatback. The seatback was then manually reclined until the volunteer was able to re-grip the steering wheel while keeping their elbows extended. All driver seat reference points and all bony landmarks were then re-measured with the volunteer in the reclined position. Then the volunteer was returned to the upright position and this marked the end of the first trial. Before starting the second trial, the reference points on the fixed stationary object independent of the buck were measured again to ensure the origin of the MicroScribe had not shifted. The volunteer was measured in the upright and reclined position for a total of three trials to quantify measurement variability. The average orientation was determined by adding each Euler rotation separately and dividing by the total number of volunteers.

1.A.2 Glenohumeral Joint Alignment in the Driving Position

The second objective of experiment A was to obtain the internal geometry of the scapula and humerus based on the average orientation of the human volunteer measurements. The right upper extremity of the 47-year-old female cadaver (height of 155 cm and weight of 57 kg) was thawed for 12 hours prior to dissecting the specimen free

of skin, subcutaneous tissue, and muscles, with the exception of the capsule, glenohumeral ligaments, and the rotator cuff muscles and tendons. During dissection, the specimen was macroscopically screened for rotator cuff or joint capsule tears. The specimen was kept moist with 0.9% normal saline throughout dissection, preparation, and testing [59].

Test preparation began by detaching the forearm from the elbow by disarticulating the olecranon of the ulna as well as the head of the radius from the condyle of the humerus. Then an aluminum rod was inserted into the medullary canal of the humerus after drilling from the center of the humeral condyle until approximately mid shaft. The aluminum rod was secured with two crossing interlocking screws. Small reference screws were then drilled into the bony landmarks of the scapula and humerus in the same location that were palpated during the human volunteer measurements. The origin of each rotator cuff muscle was then dissected from the scapula. Using a running Krackow stitch technique, one to three threads were sutured parallel with the fiber direction of each muscle until the threads reached just proximal to each musculotendinous junction. The specimen was then refrozen for testing to begin on a separate day.

After the right shoulder specimen thawed for 12 hours, the medial border of the scapula was firmly clamped to an apparatus with 3-axes of rotation (Figure 8). Muscle loading was simulated using weights attached to wires that were directed through pullies and then tied to the muscle sutures. Each rotator cuff muscle had one to three wires, and each wire had 5 N of tension applied parallel with the muscle fiber direction. To keep the humeral head physiologically flush with the glenoid fossa, a total balanced muscle load of 40 N (Table 2) was applied across the glenohumeral joint [60]. Humeral elevation and internal rotation

Table 2: Distribution of total load applied to each rotator cuff muscle. Each wire had a 5 N weight attached, which was then tied to the muscle sutures. A total of 40 N was applied to the rotator cuff.

	Teres Minor (TM)	Infraspinatus (ISP)	Supraspinatus (SSP)	Subscapularis (SUB)
Muscle Load	5 N	10 N	10 N	15 N

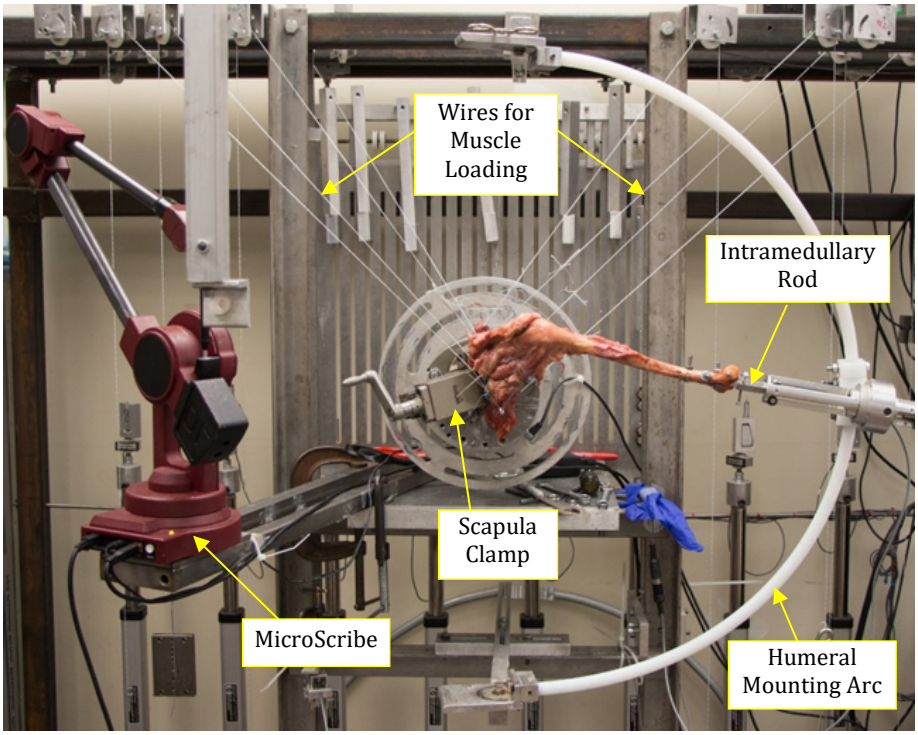

Figure 8: Lab setup for positioning the scapula and humerus in the upright and reclined positions based on the average orientation of the human volunteer measurements.

was maintained by mounting the intramedullary rod of the humerus to the plastic mounting arc (Figure 8). The scapula clamp was marked with one degree increments for each of the three axes of rotation. To orient the specimen in the average position from the volunteer results, the scapula needed to first be posteriorly tilted because the clamp's rotation about this axis is limited to one fixed plane (parallel with the vehicle X-axis), then the clamp needed to be rotated upward before internally rotating the clamp because the clamp's internal rotation does not affect the upward rotation axis.

The small screw reference points placed at the scapula bony landmarks were measured with the MicroScribe to confirm the scapula was oriented correctly. The lateral and medial

epicondyle of the humerus was measured with the MicroScribe to confirm the humerus was also oriented correctly. The same global coordinate system used during the volunteer study was also used within the specimen lab (X-axis to the front, Y-axis to the right, Z-axis downward parallel with gravity). The bony landmarks were measured while the specimen was in the average orientation for the upright position and the reclined position.

With the cadaver's right shoulder in position, Experiment B was completed first while the specimen was still intact. Then after Experiment B was completed, the right shoulder was thawed before all soft-tissue was removed from the scapula and humerus. Using the MicroScribe, each bone was digitized by taking 6,700 and 4,100 points along the bone surface of the scapula and humerus respectively, thereby creating a point cloud of each bone. Key landmarks were marked during the digitization process, which include the scapula and humeral bony landmarks used during the volunteer study as well as key bony landmarks for quantifying glenohumeral joint alignment. These include: the center of the glenoid fossa (Figure 9A), the superior glenoid rim (SGR), the humeral head apex (HHA), the humeral head center (HHC) and the bicipital groove. The HHA (Figure 9B) was calculated based on the maximum perpendicular distance from the HHC of the outermost

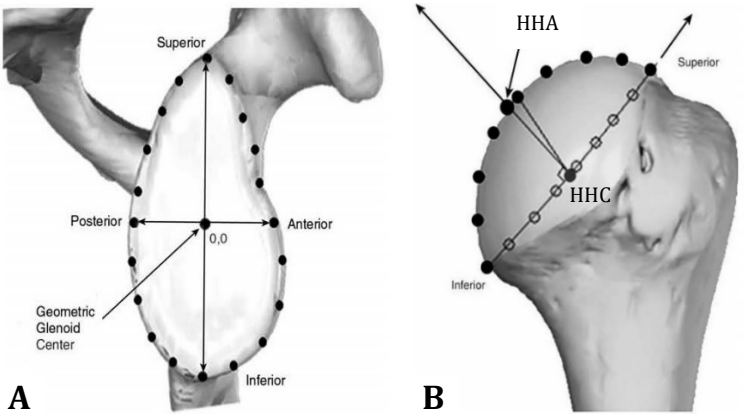

Figure 9: Landmarks of humerus and glenoid for glenohumeral joint alignment [61]. **(A)** The glenoid center is the midpoint between the superior and inferior glenoid rim. **(B)** The humeral head apex (HHA) is the maximum perpendicular distance from the center (HHC) of the border of the heads' articular cartilage.

perimeter of the articular surface [57]. The center of the glenoid fossa was the point on the surface of the cavity perpendicular to the midpoint between the superior glenoid rim (SGR) and the inferior glenoid rim (IGR). A digital mesh was then wrapped around the cloud of points to create 3D bone structures of the scapula and the humerus.

With the 3D scapula and humerus in position, joint alignment was calculated in terms of projection angles (Figure 10) between the bony landmarks of the glenoid and humeral head. The projection angles between the vector from root of the scapula spine to the SGR (V1) and the SGR to the proximal region of the bicipital groove (V2) were determined in the glenoid coordinate system (GCS) as well as the vehicle coordinate system (VCS). The projection angles between V1 and the vector parallel with the humeral shaft (V3) were also determined. The location of the HHA and HHC relative to the center of the glenoid fossa was calculated in the GCS. The angle between the anterior/posterior plane of the GCS and the sagittal plane (X-direction in VCS) was also calculated.

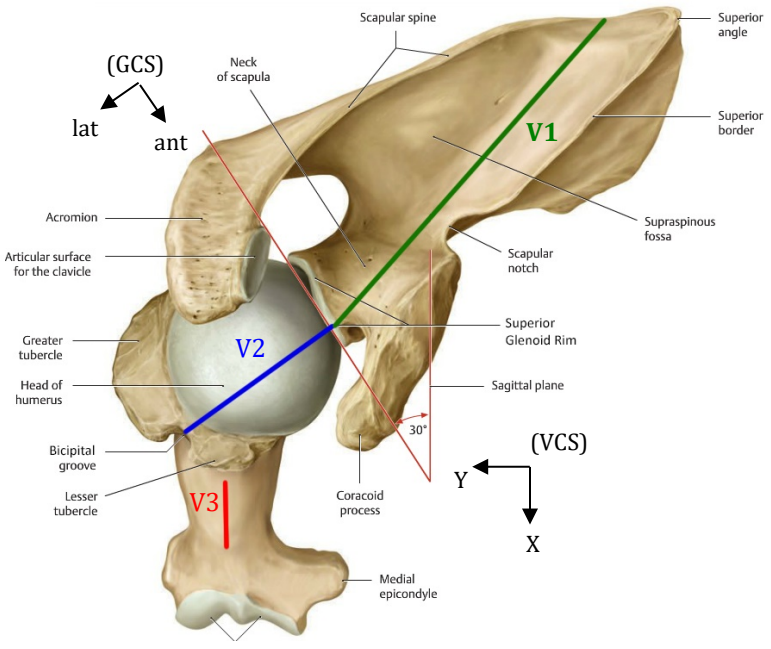

Figure 10: Anterosuperior view of the vectors quantifying glenohumeral joint alignment (adapted from [62]). Alignment shown is based on an arm hanging down by the side. V1 = scapula spine root to the superior glenoid rim (SGR). V2 = SGR to the proximal bicipital groove. V3 = parallel with humeral shaft.

Experiment B:

1.B.1 Change in Supraspinatus Muscle and Tendon Length

Additional specimen preparation was needed to measure the change in length of the rotator cuff muscles and tendons before and after humeral head displacement. First, the anterior half of the acromion needed to be removed to gain access to the SSP tendon. Prior to cutting the anterior acromion, three reference screws on the anterior acromion were measured to digitally reconstruct its intact position at a later time. After reference screws on the coracoid were measured, then the coracoid was removed to gain access to the superior border of the SUB tendon. Removal of the acromion and coracoid required cutting the coracohumeral (CH) ligament and the coracoacromial (CA) ligament.

Reference points for measuring rotator cuff tendon border length were created by suturing 1.8 mm OD glass beads to the borders of the tendon insertion, midpoint, and musculotendinous junction (Figure 11). Muscle border length was the distance from the musculotendinous junction to the muscle origin in a span of two to three points (Figure 11). The borders of the rotator cuff include the inferior teres minor (inf TM), the inferior infraspinatus (inf ISP), the superior infraspinatus (Sup ISP), the posterior supraspinatus

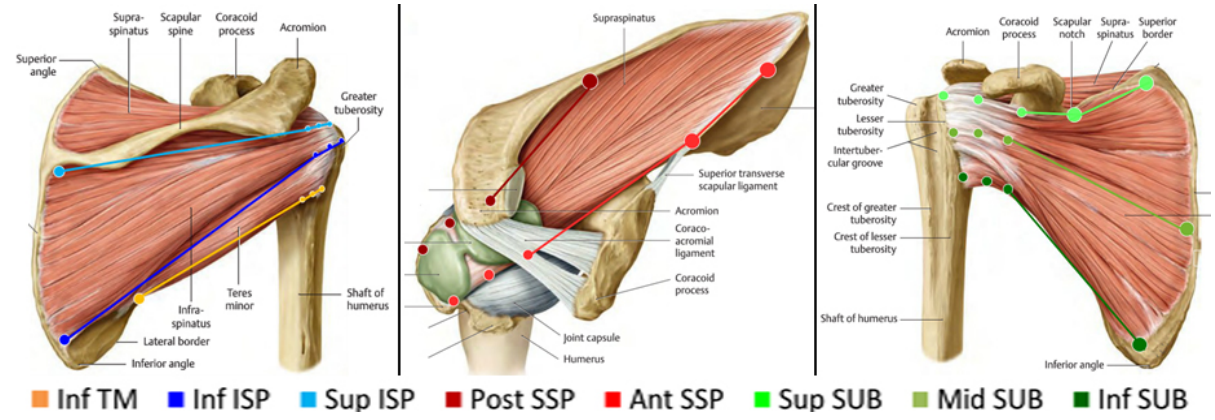

Figure 11: Diagram of points used to measure muscle and tendon length (adapted from [21]). The rotator cuff muscle and tendon border lengths include three tendon points and one to two muscle points.

(Post SSP), the anterior supraspinatus (Ant SSP), the superior subscapularis (Sub SUB), the middle subscapularis (Mid SUB), and the inferior subscapularis (Inf SUB). The specimen was then oriented using the scapula clamp into the average reclined position measured in the volunteers. While in the reclined position, the MicroScribe was used to measure the border length with the humeral head physiologically flush with the glenoid (referred to as R-neutral position).

Based on the tensile and compressive loads measured at the steering column during a rear-end collision [27], there might be some anterior displacement of the humeral head as the driver rotates rearward and some posterior displacement of the humeral head as the driver rebounds forward towards the initial upright position. There might also be inferior and superior component to the humeral head displacements during the collision. Therefore, in the reclined position the humeral head was manually translated anteriorly in the following three directions (Figure 12 green arrows): parallel with the forearm (R-fa), parallel with the lab horizontal (R-hzn), and parallel with the arm (R-arm). Humeral head displacement was locked for border measurements by tying three perpendicular

Table 3: Average ± standard deviation of humeral head translation (mm) in each of the different displaced positions.

	Reclined	Upright
fa	13.5 ± 1.4	14.4 ± 0.8
hzn	14.4 ± 1.3	20.3 ± 0.6
arm	16.7 ± 1.2	12.5 ± 1.2
dwn / up	20.6 ± 2.5	10.0 ± 3.2

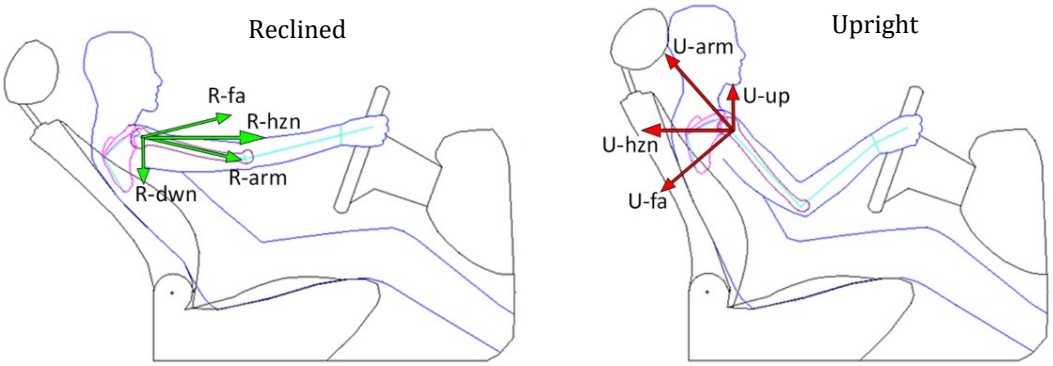

Figure 12: Illustration depicting the direction of humeral translations applied to the cadaver while the specimen was oriented in the average reclined and upright position.

wires to the humerus and clamping them to surrounding fixed objects. For the upright position, the humeral head was translated posteriorly (Figure 12 red arrows) using the same three references (U-fa, U-hzn, U-arm) but in the opposite direction. The humeral head was also translated vertically downward in the reclined position (R-dwn) and upward in the upright position (U-up). Since low-speed rear-end collisions typically do not result in dislocation of the arm, the magnitude of humeral head displacements (Table 3) was limited to a point where the compressive load of the rotator cuff muscles would return the humeral head to the glenoid fossa upon release. Displacements of the humeral head were repeated three times to quantify variability in repeating the displaced positions.

1.B.2 Passive Tightness of the Supraspinatus Muscle

To determine the relative tightness of the rotator cuff muscles, the rotator cuff border lengths with the humeral head in the neutral and displaced positions were compared with border lengths at its limit in range of motion (ROM). Muscle tightness was defined based on the difference between its current length to the length when the specimen was positioned at its maximum ROM. In other words, the closer the difference in length is to zero, the closer the muscle length is to ROM limit. The specimen's limit of humeral axial rotation (Figure 13) was defined as 2 Nm of torque resistance [57]. The humerus elevation was iteratively adjusted until max muscle length was measured. The same balanced rotator cuff muscle load of 40 N was used with the specimen at ROM limit.

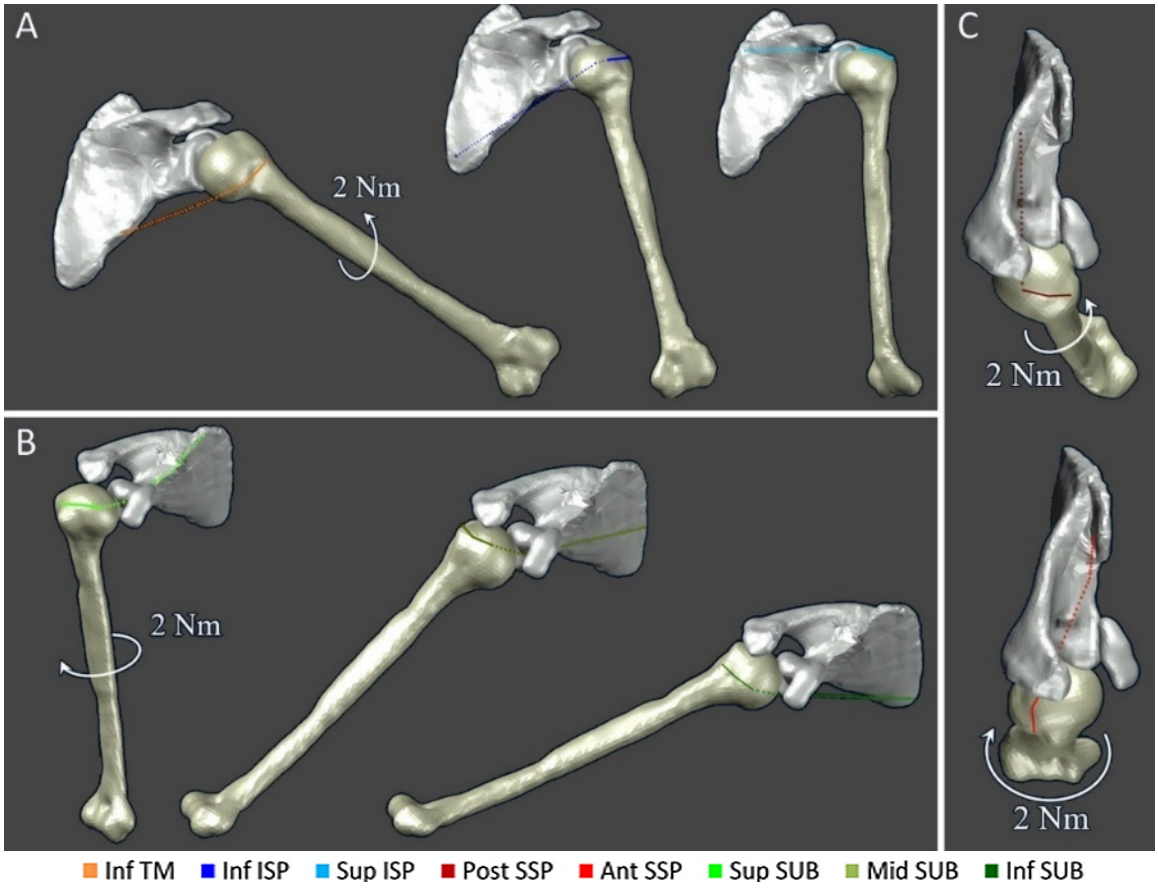

Figure 13: Positions of the specimen at maximum physiological range of motion (ROM). Dashed line is muscle and solid line is tendon. The ROM limit positions are: **(A)** TM and ISP, **(B)** SUB, and **(C)** SSP.

1.B.3 Supraspinatus Tendon Impingement

SSP tendon impingement with the acromion was examined during humeral head displacement. Contact between the SSP tendon and the acromion was visually identified while the acromion was intact, but the SSP tendon location during contact could not be measured until after the anterior acromion was cut. The SSP tendon was measured while the humeral head displacement was obstructed by the posterior acromion. The location of the SSP tendon in relation to the full acromion was determined after digitally adding the anterior acromion to the posterior acromion.

1.B.4 Supraspinatus Tendon Loading to Failure

Tensile testing of the SSP tendon was conducted using an Instron machine (Instron Co., Canton, MA, USA). Some preparation was required prior to tensile testing. The contralateral (left) shoulder of the same cadaver was used for tensile testing rather than the right shoulder to avoid the effects of repeated freeze-thaw cycling, which can significantly reduce the tendon's ultimate load, stiffness, ultimate stress and Young's modulus [63], and because tensile testing runs the risk of causing bone damage to the specimen. Therefore, the right shoulder was returned to the freezer for completion of bone digitization process of Experiment A on a later day. The protocol for dissection and preparation of the left shoulder was the same as that described for the right shoulder in Experiment A.

Since differences in glenohumeral alignment may have an effect on SSP tendon strain [64], the orientation of the SSP muscle and tendon relative to the proximal humerus while in a forward flexed position (like that when holding a steering wheel) was determined before using the Instron. The left scapula was positioned using the scapula clamp and the humerus was mounted to the arc to orient the specimen in the reclined position. Three screws were added to the proximal humerus to quantify humeral orientation independent of the epicondyles while the specimen was in the reclined position. The anterior acromion was cut so that the proximal region of the SSP tendon could be measured.

After the orientation measurements were obtained, the specimen was removed from the scapula clamp and the humerus was disarticulated from the scapula by cutting the capsule along the entire glenoid rim. Then the intramedullary rod was removed from the humeral shaft. Then the humeral shaft was cut approximately six inches distal to the

surgical neck. The distal end of the 6-inch humeral shaft was then potted using bone cement to allow for humeral fixation to the Instron base. Care was taken not to cement the humerus over the three proximal reference screws needed to orient the humerus correctly relative to the axis of the Instron, i.e., muscle direction of pull.

The SSP muscle was clamped to the Instron just proximal to the musculotendinous junction (Figure 14). The SSP tendon was only dissected free from the ISP from the musculotendinous junction to the midpoint of the tendon, but remained intact with the ISP from the midpoint to the insertion to keep the distal SSP as intact as possible. Furthermore, the superior capsule was not dissected from the articular side of the SSP. The humerus was then oriented so that the Instron's vertical pull of the SSP muscle would be equivalent to the direction of pull when the humerus was in a forward flexed position—putting the SSP tendon in a slight anterior curved configuration relative to the direction of muscle pull. Just prior to tensile testing, the clamp was frozen using liquid nitrogen to improve grip on the musculotendinous junction. Then the specimen was preconditioned with three cycles of tensile loading from 0 to 200 N. The tendon length at the end of the three cycles was measured during a pre-load of 5 N. Then a video digitizing system (Canon 3CCD Digital Video Camcorder GL2 and WINanalyze 2D v1.9) with an accuracy within 0.46 mm was used to measure the change in proximal and distal tendon length on the bursal side as the specimen was loaded to failure at a rate of 0.83 mm/s.

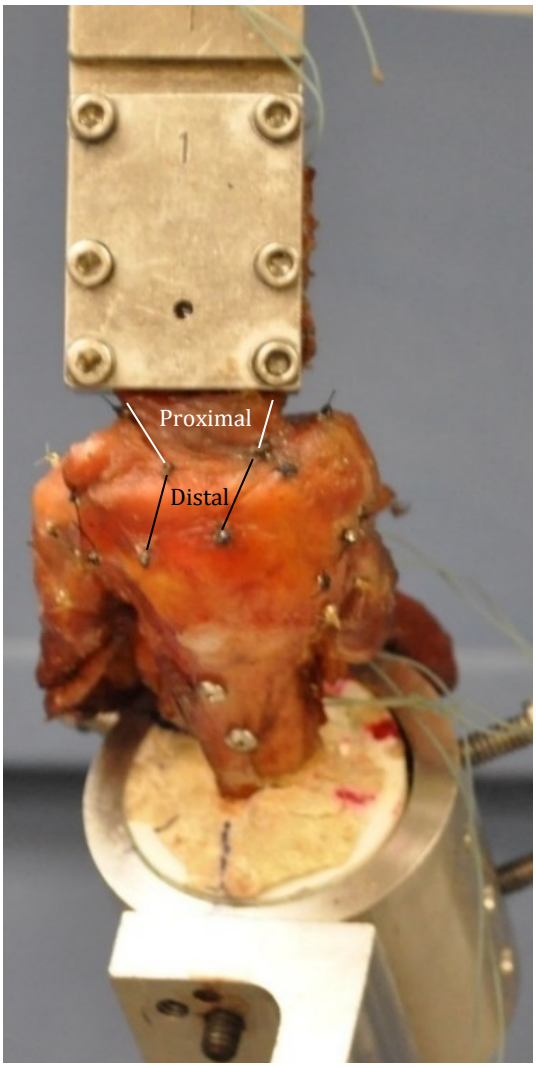

Figure 14: SSP tensile test configuration prior to loading the specimen to failure.

CHAPTER 2: Results

Experiment A:

2.A.1 Scapula and Humerus Orientation of Volunteers in the Driving Position

The scapula and humerus orientation (Table 4) of volunteers holding a steering wheel at 10 and 2 o'clock was determined relative to the vehicle coordinate system (Figure 15). For example, the scapula orientation in the upright position was 9 ± 7° posterior tilt (PT), then 9 ± 4° upward rotation (UR), then 42 ± 6° internal rotation (IR). Additional equivalent Euler angle rotation sequences for the scapula can be found in Appendix B. For both the upright and reclined positions, the repeated trials had an average standard deviation of 3 ± 1° PT, 2 ± 1° UR, 2 ± 1° IR for the scapula, and 1 ± 1° HA, 2 ± 1° Elev, 3 ± 2° IR for the humerus. The average seatback angle in the reclined and upright positions were 44 ± 3° and 28 ± 1° respectively (equivalent to 38 ± 3° and 22 ± 1° without the foam block). Volunteers set the driver seat 169 ± 53 cm rearward from the full forward position.

Table 4: Average ± standard deviation of the scapula and humerus orientation in the driving position. Scapula Euler angle sequence: posterior tilt (PT), upward rotation (UR), and internal rotation (IR). See Appendix B for alternative sequence. Humerus Euler angle sequence: horizontal adduction (HA), forward elevation (Elev), and internal rotation (IR).

Seat Position	Scapula			Humerus		
	PT	UR	IR	HA	Elev	IR
Reclined	21±7°	8±4°	45±5°	2±3°	78±5°	28±12°
Upright	9±7°	9±4°	42±6°	0±5°	56±4°	11±6°

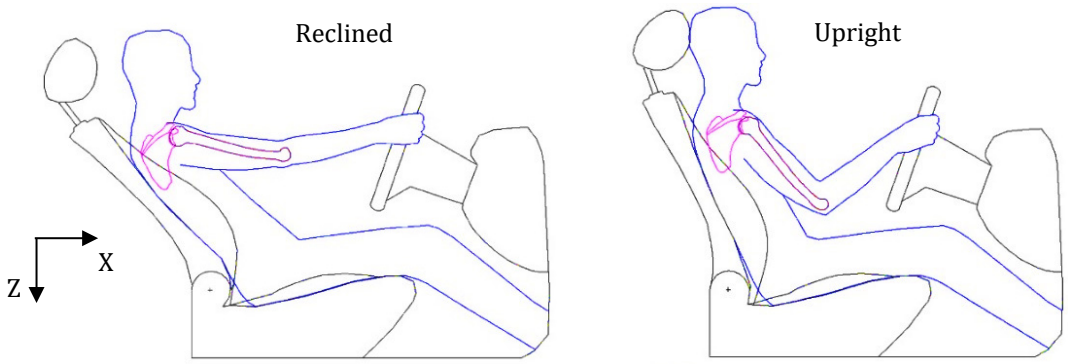

Figure 15: Illustration of scapula and humerus while in the reclined and upright position. Note that this illustration is based on the orientation of the author's bony landmarks, not the average of the volunteer data.

2.A.2 Glenohumeral Joint Alignment in the Driving Position

The scapula and humerus of the cadaver was oriented in the reclined and upright position based on the average values from the volunteer results (Figure 16A&B). For example, in the reclined position the scapula was oriented 21° PT, 8° UR, 45° IR and the humerus was oriented 2° HA, 78° Elev, 28° IR. The orientations of the upright and reclined positions were then quantified relative to bony landmarks near the glenohumeral joint (Table 5). For example, in the reclined position the vector V2 (Figure 17A) was 25° posterior and 0° inferior to vector V1 in the glenoid coordinate system (GCS); which corresponds with 25° to the right and 50° above V1 in the vehicle coordinate system (VCS). In addition, vector V3 was 30° anterior and 30° inferior of V1 in the GCS.

The deep internal glenohumeral geometry was quantified in terms of the bony landmarks of the humeral head with respect to the glenoid (Table 5). For example, while in the reclined position the humeral head apex (HHA) was 4 mm anterior and 1 mm inferior to the glenoid center (Figure 17A) in the GCS, and the humeral head center (HHC) was 4 mm anterior and 3 mm inferior to the glenoid center in the GCS. The angle between anterior/posterior plane of the GCS and the plane parallel with the X-direction of the VCS (sagittal plane) was approximately 45° for the reclined and upright positions.

In the upright position, it was noted that the proximal bicipital groove was coincidentally aligned with the anterior edge of the acromion, which has been defined as external axial rotated position of the humerus in previous biomechanical cadaveric studies [57]. It was also noted that the SSP Muscle near the musculotendinous junction slid down the scapula neck to the 9 to 10 o'clock region of the glenoid rim as the arm was forward flexed to the upright and reclined positions (Figure 17B).

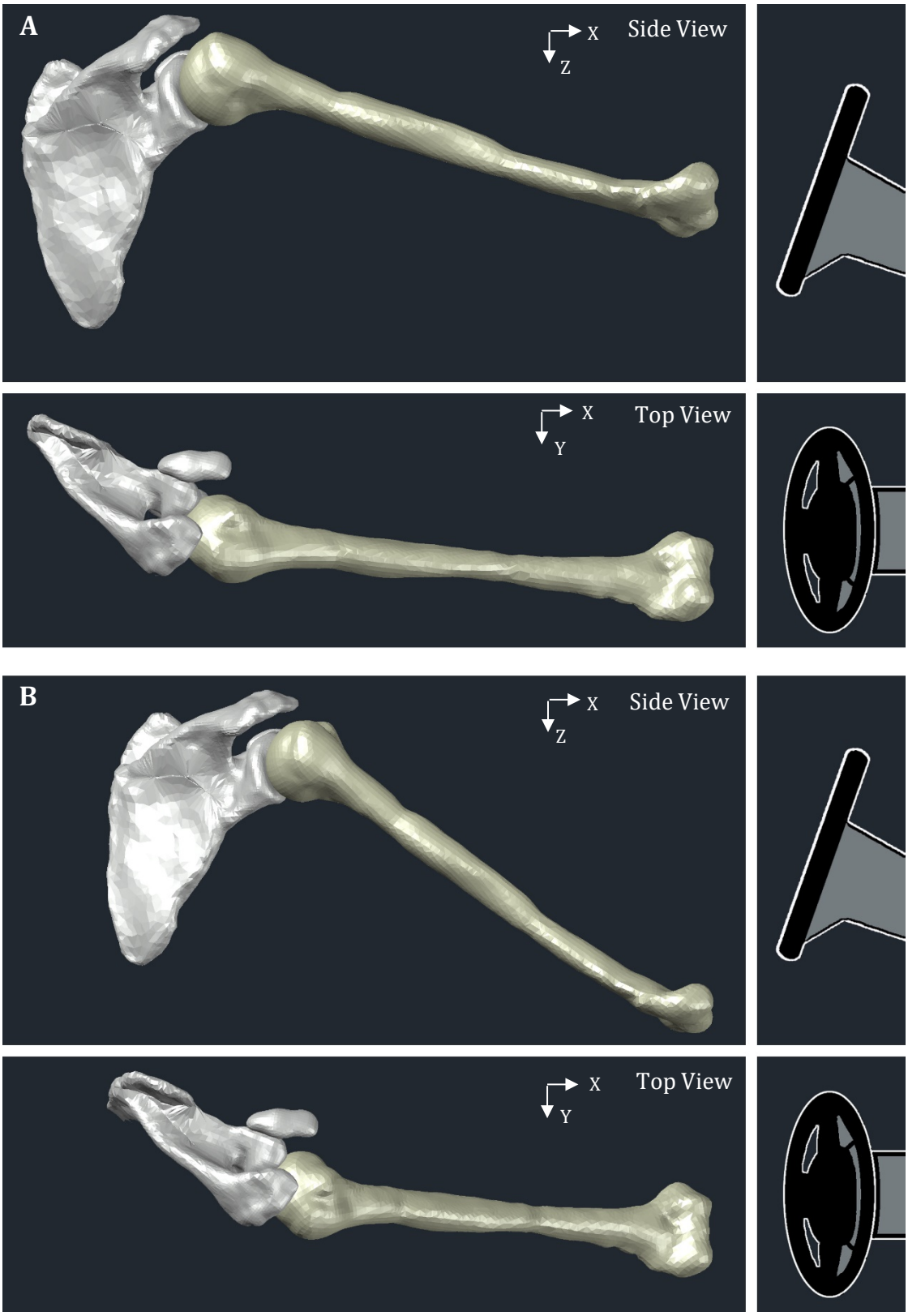

Figure 16: Digital model of the scapula and humerus in relation to the steering wheel for the **(A)** reclined position and **(B)** upright position. Perspective based on the vehicle coordinate system (VCS).

Table 5: Orientation of the glenohumeral joint in the driving position in terms of projection angles between vectors defined by bony landmarks and based on the position of the humeral head on the glenoid fossa. V1 = vector from the root of the scapula spine to the superior glenoid rim (SGR). V2 = vector from the SGR to the proximal bicipital groove. V3 = vector parallel with humeral shaft. The location of the humeral head apex (HHA) and humeral head center (HHC) is relative to the glenoid center. Dimensions provided in the glenoid coordinate system and in parenthesis is vehicle coordinate system. Angles rounded to nearest 5 degrees.

	Reclined	Upright
V2 ∢ V1	25° posterior, 0° inferior (25° right, 20° up)	30° posterior, 10° inferior (35° right, 20° up)
V3 ∢ V1	30° anterior, 30° inferior (20° left, 40° down)	40° anterior, 40° inferior (15° left, 50° down)
HHA	4 mm anterior, 1 mm inferior	0 mm anterior, 2 mm inferior
HHC	4 mm anterior, 3 mm inferior	1 mm anterior, 0 mm inferior

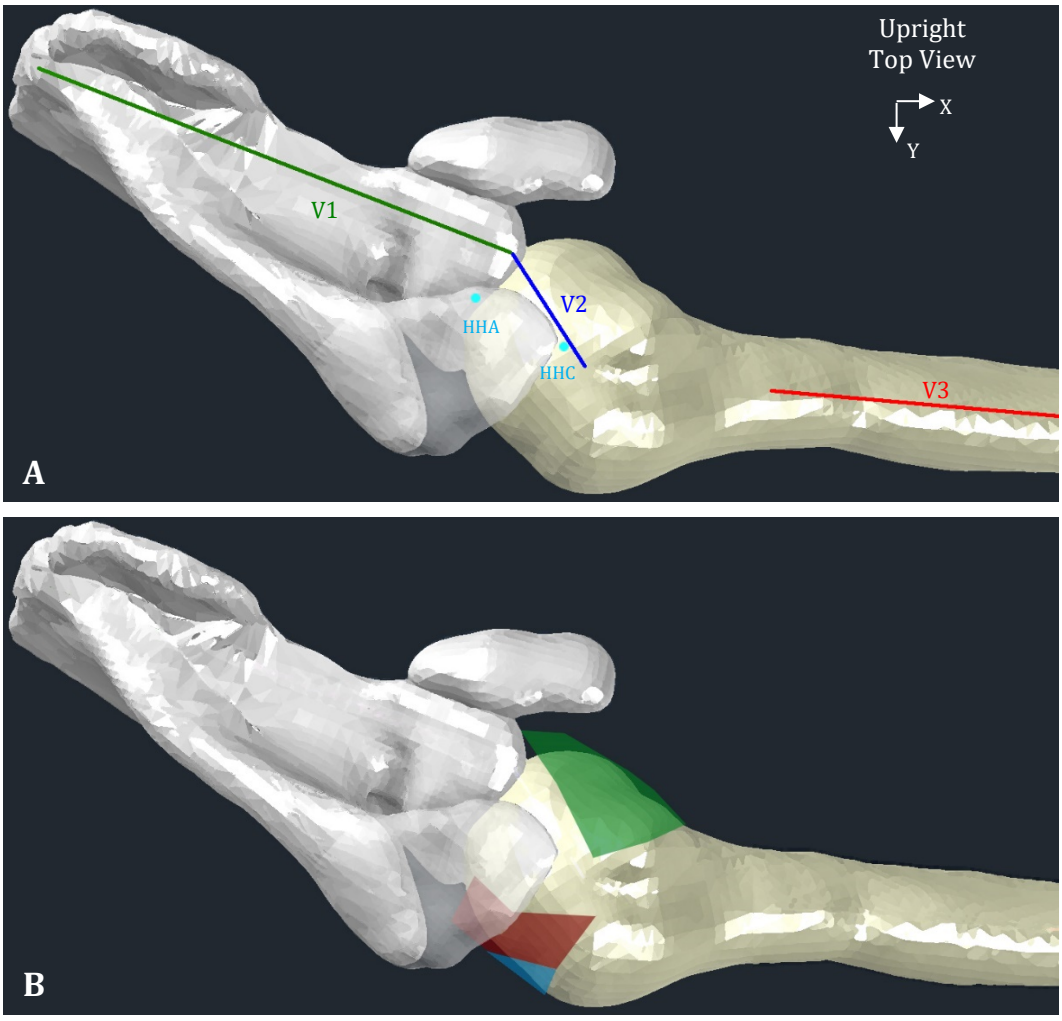

Figure 17: (A) Orientation of humerus relative to the scapula based on projection angles between vectors V1, V2, and V3. **(B)** Location of SSP tendon (red) from musculotendinous junction to insertion. Also shown are the SUB tendon (green) and the ISP tendon (blue).

Experiment B:

2.B.1 Change in Supraspinatus Muscle and Tendon Length

The SSP muscle had the largest increase in length relative to other rotator cuff muscles for the following displaced positions: R-hzn, R-arm, R-dwn, U-fa, U-hzn (Figure 18). It was not possible to rank the SSP tendon elongation relative other rotator cuff tendons due to the fact that the minimal changes in tendon length were within the standard deviation of repeated displacement trials and MicroScribe measurement accuracy (Figure 18).

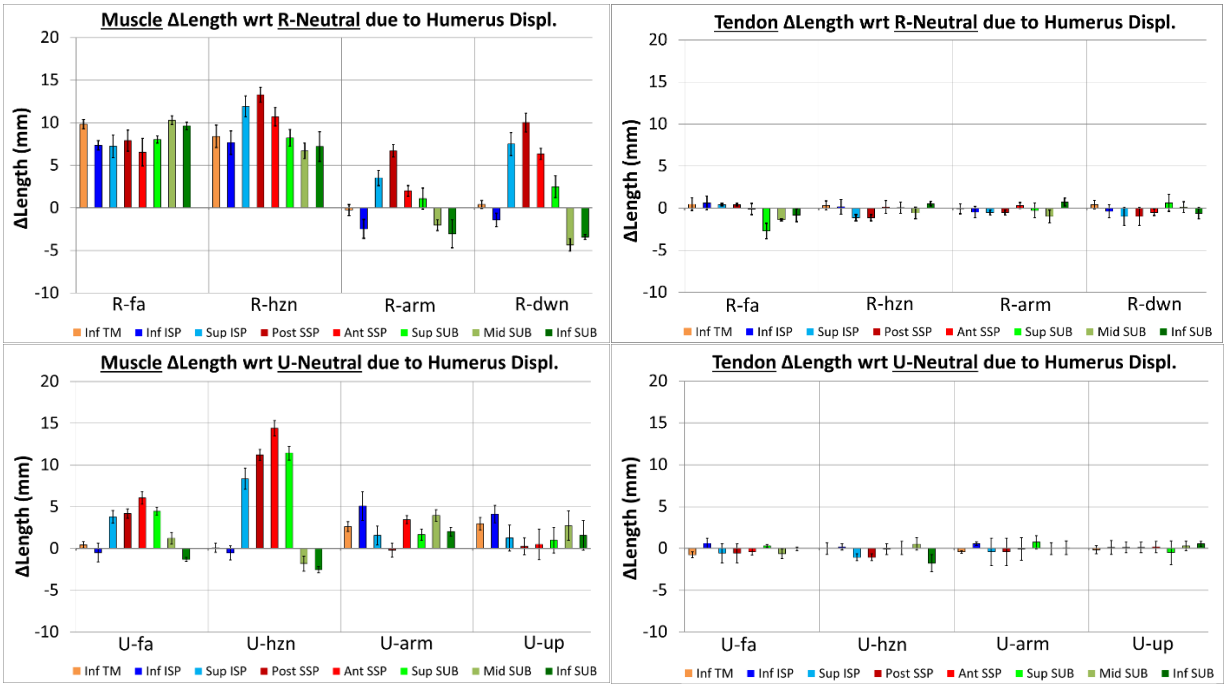

Figure 18: Change in length of rotator cuff borders due to humeral head displacement. There were displaced positions in both the reclined and upright positions in which the SSP muscle elongated the most. SSP tendon elongation could not be ranked relative to other tendons due to minimal changes in tendon length. Flush alignment of the humeral head with the glenoid fossa is abbreviated R-Neutral and U-Neutral for the reclined and upright positions respectively.

2.B.2 Passive Tightness of the Supraspinatus Muscle

The length of the SSP muscle when the specimen was in the reclined neutral (R-neutral) position was less than the length of the SSP muscle at ROM limit (Figure 19). For example, the anterior supraspinatus (ant SSP) muscle border in R-neutral was shorter than the

anterior SSP length at ROM limit by 12 ± 1 mm, and the posterior SSP (post SSP) muscle border was less than the length at ROM limit position by 19 ± 1 mm.

The lengths of the SSP muscle in the displaced positions were less than the length in the ROM limit position for all displacements except U-hzn. The length of the ant SSP border in the U-hzn position was longer than the ROM limit length by 8 mm.

The length of the SSP muscle was closest to its ROM limit length compared to other rotator cuff muscles in all positions, i.e., the SSP muscle was tighter than the other rotator cuff muscles in all positions.

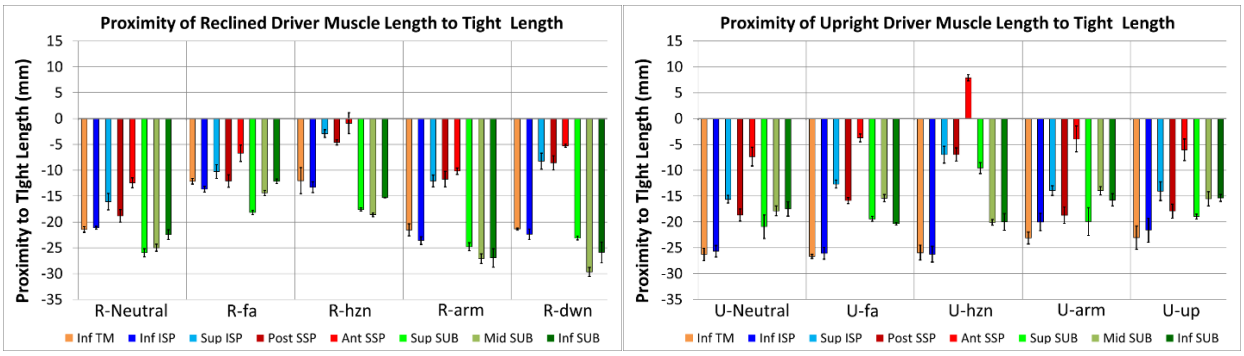

Figure 19: Difference between rotator cuff lengths in the driving position vs ROM limit positions. The closer the difference in length is to zero, the closer the muscle length is to ROM limit, i.e., the tighter the muscle. Positive values represent muscle lengths greater than the ROM limit muscle length. The SSP was the tightest muscle in both neutral positions and in all displaced positions.

2.B.3 Supraspinatus Tendon Impingement

Anterior and inferior translation of the humeral head had no bony obstructions from the scapula (Figure 20A green arrow). Posterior translation was deflected laterally by the glenoid fossa (Figure 20A red arrow) and obstructed by the acromion if there was a superior translation component (Figure 20B). There was impingement of the proximal SSP tendon with the mid region of the acromion in the U-up and U-arm positions (Figure 20C red tendon). There was no impingement of the distal SSP tendon.

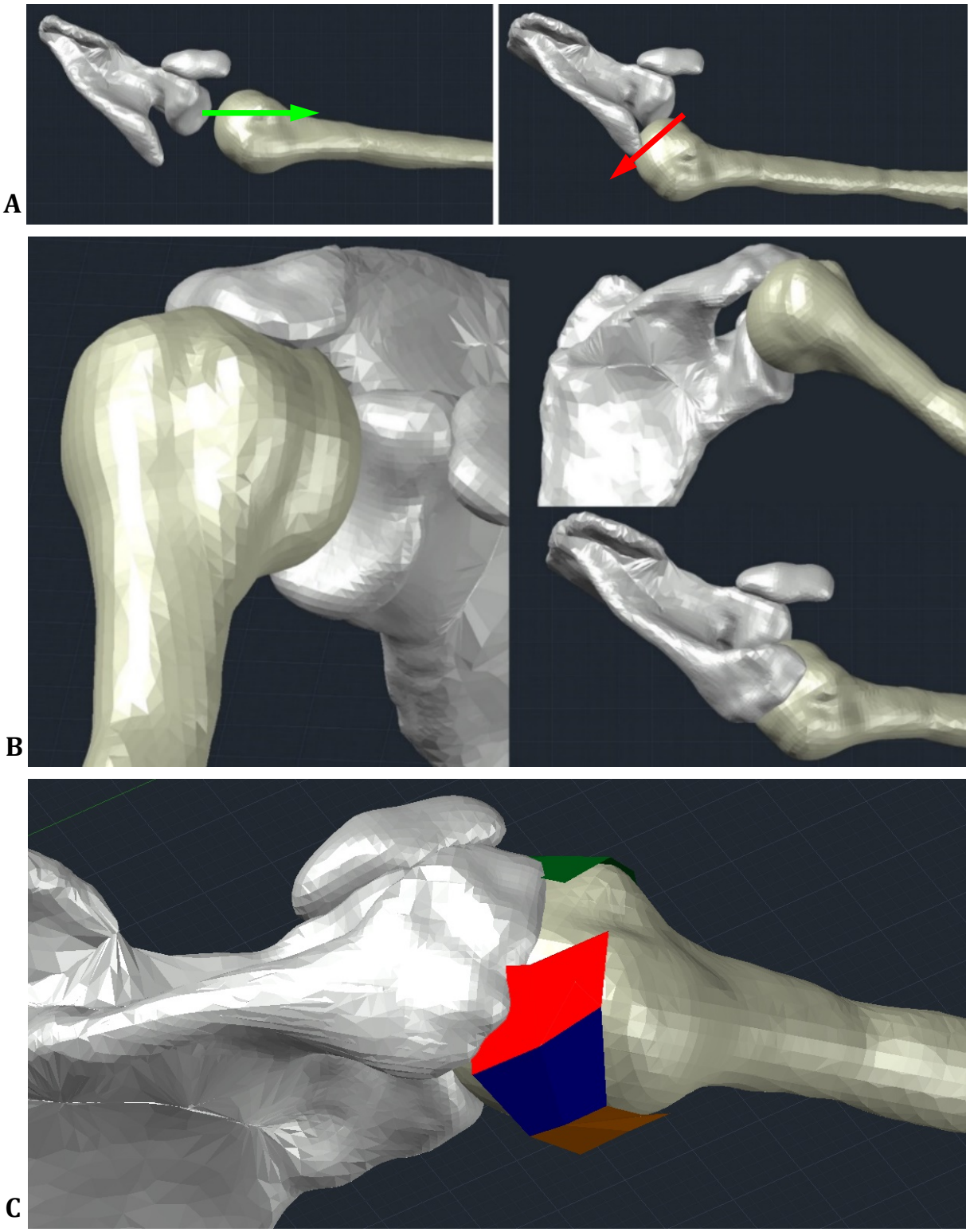

Figure 20: View of bony obstructions during humeral head displacement. **(A)** Example of no obstruction with anterior displacement (green arrow) and example of lateral deflection with posterior displacement (red arrow), note: anterior acromion removed to show glenoid fossa. **(B)** Example of obstruction of the humeral head with the acromion during posterosuperior translation (U-arm position). **(C)** Alignment of the SSP tendon (red) with the acromion in the U-arm position. Green = SUB, Blue = ISP, Orange = TM.

2.B.4 Supraspinatus Tendon Loading to Failure

The proximal humerus fractured superior to the surgical neck while the SSP tendon was loaded to 904 N of tension. The fracture occurred 20 seconds after the start of loading to failure. The posterior SSP at the musculotendinous junction near the clamp started to tear at 600 N. On the bursal side of the tendon, the final strain for the proximal half was approximately 11%, whereas the final strain for the distal half was approximately 2%. The distal supraspinatus did not have any visual bursal-sided tears. The superior capsule also remained intact. The articular side of the distal SSP tendon was confirmed not to have any macroscopic tears after dissecting the superior capsule free from the SSP tendon.

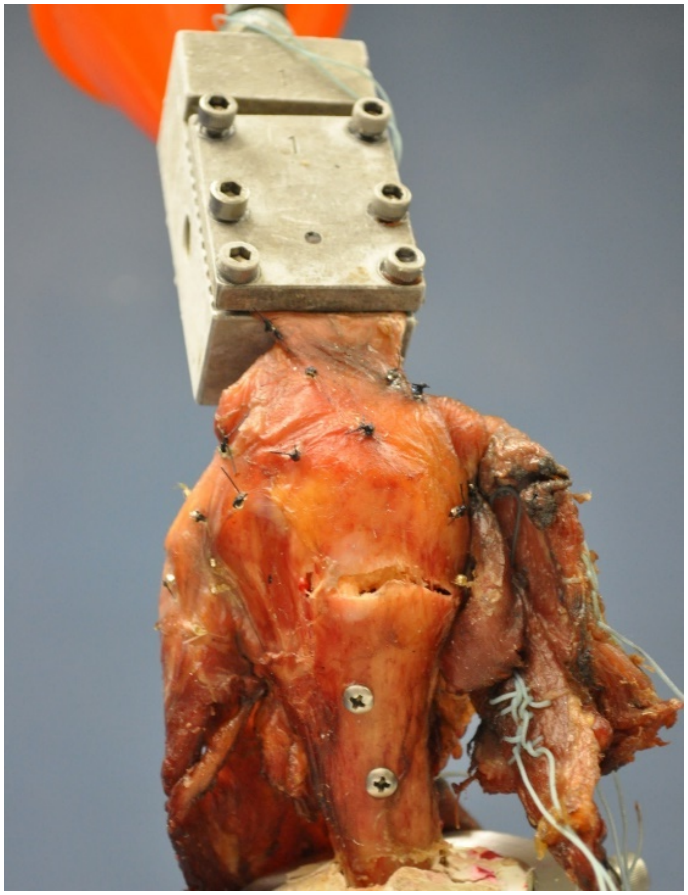

Figure 21: The proximal humerus fractured when the SSP tendon was loaded to 904 N of tension. The distal region of the SSP tendon did not tear.

CHAPTER 3: Discussion

Experiment A:

3.A.1 Scapula and Humerus Orientation of Volunteers in the Driving Position

The standard deviation of scapula orientation was low (≤7°), consistent with the hypothesis, despite the large range in volunteer height (145 – 191 cm); most likely because shorter volunteers sat closer to the steering wheel than taller volunteers—resulting in similar recline angles (44 ± 3°) even with large difference in seat forward/aft positions (169 ± 53 cm). The Euler rotation angles and standard deviation of the scapula were consistent with previous studies on elevating the arm near the sagittal plane in different body position scenarios [48, 50, 65-69]. The scapula in the reclined position had greater posterior tilt, similar upward rotation, and a little more internal rotation compared to the upright position. The humerus had greater elevation and internal rotation while in the reclined position compared to the upright position. The standard deviation for the orientation of the humerus was less than ≤6°, for all Euler rotations except for internal rotation (12°)—most likely because the elbow was the least constrained region of the upper extremity when volunteers held onto the steering wheel. Internal rotation of the humerus also had the highest inter-subject standard deviation of 3 ± 2° during repeated trials—most likely due to the lack of constraint at the elbow and the proximity of the epicondyles.

The effects of using the foam block to provide a small amount of space for the MicroScribe stylus and for palpation was investigated prior to the first volunteer. During the investigation, the foam block was kept loosely against the seatback without any fixation. As the driver was seated against the foam block, the abdominal muscles were

tightened, the foam block was removed, and the seatback was tilted forward until contact with the driver's back was reestablished and abdominal muscles relaxed. During this process, minimal scapula motion was palpated as the driver maintained their arm elevation and grip on the steering wheel.

The main limitation of the first part of Experiment A was that all volunteers were measured in static positions, but a rear-end collision is a rapid dynamic event in which the driver translates rearward relative to the seat and firmly presses up against the seatback prior to and during the reclining motion. None of the volunteers were forcefully pressed against their seat prior to reclining, therefore the reclined position is an approximation to the motion in an actual collision. Measuring the volunteers in an upright and reclined position does not capture all possible positions of the scapula and humerus during a collision, but it does approximate the alignment when peak steering wheel loads occur, and it does give an approximation of the maximum range of change in scapula-humerus alignment during a low-speed rear-end collision for drivers who maintain grip on the steering wheel.

3.A.2 Glenohumeral Joint Alignment in the Driving Position

Projection angles of the vectors between the humerus and scapula near the glenohumeral joint allow for future studies to position a specimen without having to preserve the epicondyles of the humerus. In addition to orienting the humerus, the location of the proximal region of the bicipital groove relative to the superior rim of the glenoid also provides information for the orientation of the long head of the biceps tendon in the driving position, which may be useful for future studies on labral injury analysis, such as a superior labrum anterior to posterior (SLAP) tear. Furthermore, the bicipital groove is a

landmark to help visually separate the SSP tendon insertion (greater tuberosity) from the SUB tendon insertion (lesser tuberosity) for rotator cuff injury analysis [70].

The specimen's alignment of the bicipital groove with the anterior edge of the acromion was consistent with the arm being in external axial rotation [71] when holding a steering wheel at the 10 and 2 o'clock position. Furthermore, this specimen's angle of 45° between the anterior/posterior plane of the GCS and the sagittal plane is consistent with protracting the shoulders while holding the steering wheel (typically 30° when the arm is hanging down by the side, but can range from 5° to 60° depending on shoulder protraction [62]).

A limitation to this portion of the study is that only one specimen was positioned in the average orientation of the volunteer results. Quantifying the variability of the glenohumeral alignment across a variety of driver sizes would require many more specimens. One source of variability would be due to anatomical variation in the alignment of the humeral neck axis with the epicondyle axis (referred to as retroversion). Retroversion of the humeral head relative to the epicondyles has been measured to be approximately 30 ± 9° [72]. However, compared to the full range of humeral axial rotation, differences in specimen retroversion would most likely result in an overall similar alignment.

Experiment B:

3.B.1 Change in Supraspinatus Muscle and Tendon Length

The results of the displacement tests suggest that the SSP muscle can elongate more than the other rotator cuff muscles in both the reclined and upright positions during a rear-end collision. However, despite large humeral head displacements, elongation of the SSP tendon was minimal (0 ± 1 mm) in all displaced directions. In order for the SSP tendon to have undergone greater elongation, the SSP would have needed greater muscle loading.

Using Eq. 1, the SSP muscle load of 10 N can be estimated as a percentage of the muscle's maximum voluntary contraction (%MVC) [2]. Assuming a specific tension (σ) of 33 to 60 N/cm^2 [2] and a SSP physiological cross-sectional area (PCSA) of 3.5 to 7.0 cm^2 [73],

$$F = \%\text{MVC} \cdot \sigma \cdot PCSA \quad \textbf{Eq. 1}$$

then solving for %MVC based on 10 N of SSP muscle load (F) would equate to 2 to 9% MVC—which is equivalent to a relaxed volunteer. Therefore, displacement of the humeral head without dislocation and with a relaxed SSP muscle presents little risk to tear of a healthy SSP tendon.

There are several limitations to this portion of the study. The exact interaction of the humeral head with the glenoid during a low-speed rear-end collision is currently unknown. The effects of rotator cuff muscle activation as well as other shoulder muscles (such as the deltoid and latissimus dorsi) on the direction of humeral head displacement during impact makes it difficult to predict the interaction at the glenohumeral joint. This is why the humerus was translated in eight different directions. Furthermore, in vivo muscle contraction was simulated on the cadaver using weights attached to sutures via wire and pulley. Loads applied to this specimen were uniformly distributed across each rotator cuff tendon, but in a living person, muscle contraction occurs from electrical stimulation from the nervous system, which might result in non-uniform contraction of the rotator cuff and other muscles during a collision.

3.B.2 Passive Tightness of the Supraspinatus Muscle

The SSP muscle was tighter than the other rotator cuff muscles in all displaced positions, which clarifies that the SSP muscle elongations in part 1 were not due to muscle

slack. The SSP initiates abduction and will continue to shorten when the arm abduction angle increases, the ISP and TM externally rotate the arm, and the SUB adducts and internally rotates the arm [1]. In the driving position, the arm is mainly forward flexed and externally rotated with minimal abduction. Since the SSP muscle elongated the most with displacement and was the tightest SSP muscle, an activated SSP muscle and tendon may be at risk of resisting a higher portion of the external load than other rotator cuff muscles. However, for a relatively relaxed SSP muscle, the displacements of the humeral head without dislocation presents little risk to an intact SSP tendon due to the available length of muscle needed for the shoulder joint to achieve its large range of motion.

The SSP muscle length during humeral head displacement was less than the ROM limit length in all displaced positions except U-hzn. Translation of the humeral head to the posterior edge of the glenoid (U-hzn position) would have required substantially more external load to the humerus had the coracohumeral (CH) ligament (Figure 22A) not been

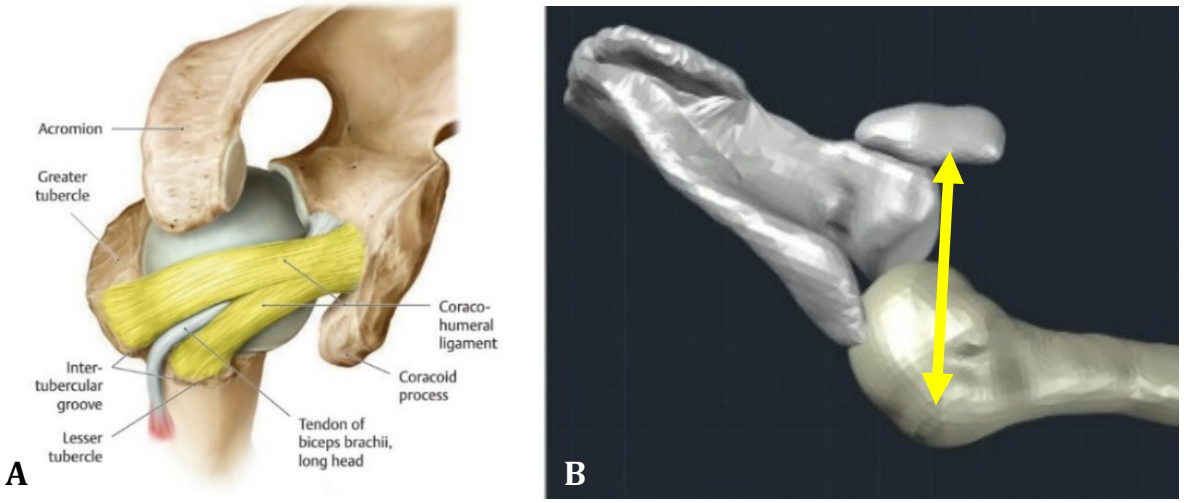

Figure 22: Depiction of how the coracohumeral (CH) ligament resists posterior translation when the arm is in forward flexion while holding a steering wheel **(A)** Location of the coracohumeral (CH) ligament (yellow) [62]. **(B)** Approximate direction in which the CH ligament resists posterior translation.

cut during removal of the coracoid, which suggests that the CH ligament may play an important role in resisting posterior dislocations. The CH ligament is known to resist inferior translation when the arm is in external rotation [1]; however, in forward flexion the CH ligament is closely in line with the direction of posterior translation (Figure 22B) and may be partially wrapped around the humeral head, thereby providing resistance to posterior translation.

This finding is consistent with the concept that ligaments play an important role in passive joint restraint at the end of shoulder range of motion [1, 2]. The lack of proximity of the rotator cuff muscles to ROM limit length also confirms that the driving position is in the mid-range of motion, which means the shoulder muscles play a bigger role in providing dynamic joint stability than the shoulder ligaments during a low-speed rear-end collision [1, 2].

3.B.3 Supraspinatus Tendon Impingement

Lack of direct contact of the distal SSP tendon with the acromion during humeral head displacement suggests that subacromial impingement may not occur to the distal SSP tendon during a low-speed rear-end collision. The limitation of this portion of the study is that the alignment of the SSP tendon with the acromion is based on holding the steering wheel at the 10 and 2 o'clock position.

3.B.4 Supraspinatus Tendon Loading to Failure

While in a forward flexed position, this specimen's SSP tendon withstood 904 N of tension without sustaining a distal tendon tear, which suggests that i) this specimen had a healthy SSP tendon, ii) a healthy SSP tendon would most likely withstand the tension produced within the limits of physiologically possible eccentric muscle contraction, and iii)

extreme tension in a healthy SSP tendon may result in bone failure rather than a distal tendon tear.

Tensile testing the SSP tendon in a forward flexed position resulted in a similar failure load as previous uniform tensile tests of specimens in an abducted position (approximately 1000 ± 400 N) [74, 75]. For comparison, maximum SSP muscle loads based on parameters used for Eq. 1 range from 115 to 350 N, which is consistent with previous published estimates [76-81]. However, currently there are no EMG studies to suggest that the SSP muscle is physiologically capable of achieving maximum muscle contraction while the arm is in a forward flexed position like that when holding onto a steering wheel. EMG measurements of volunteers performing upright chest press and row exercises had increased SSP muscle activity to approximately 30 ± 15% MVC and 15 ± 15% MVC, respectively [45].

Age-related degeneration of the SSP tendon has been shown to reduce the tendon's tolerance to failure. Previous uniform tensile tests of SSP tendons found that as the age of the tendon increased from 40 to 60 to 80 years old, the average ultimate loads dropped from 1300 N to 1000 N to 600 N [75]. Sano et al [15] histologically quantified degeneration of SSP tendons at the anterior and posterior subregions prior to testing the middle subregion to failure and found that the level of tendon degeneration was more correlated with insertion-type tendon tears. Approximately 70% of the previous uniform tensile tests of specimens in an abducted position resulted in bone failures rather than tendon tears [74, 75]; however, these previous tests had bone avulsions rather than fractures. This specimen may have fractured due to the load-sharing effect across the humeral head that occurs

during minimal arm abduction [81], as indicated by the large difference in strain between the distal half and proximal half of the SSP tendon.

Physiologically the anterior subregion of the SSP tendon may be subjected to higher loads than the posterior subregion during some arm activities based on differences in muscle and tendon cross-sectional areas [82]. Non-uniform loading has been modeled by cutting cadaveric SSP tendons into 2 to 3 separate strips [76, 83]. More than 75% of the strips tore at the insertion, and the ultimate load of the anterior strips dropped from 779 ± 218 N to 411 ± 158 N, and the ultimate load of the posterior strips dropped from 335 ± 164 N to 88 ± 32 N. The effect of non-uniform loading is similar to that of tendon degeneration in that the ultimate load of the tendon drops and therefore becomes weaker than the bone. These tests suggest that non-uniform muscle activation could be a potential mechanism for tearing a healthy SSP tendon during excessive eccentric SSP muscle contraction [76]. However, currently there are no studies to suggest non-uniform SSP muscle activation during a rear-end collision. Future rear-end collision tests of volunteers with fine-wire EMG measurements of the anterior and posterior subregions of the SSP muscle may be of value.

There is also the possibility that a driver may have a pre-existing asymptomatic SSP tendon tear that is rendered symptomatic by a rear-end collision. Previous studies have found that symptomatic tears tend to be larger than asymptomatic tears [16, 84, 85]. Rotator cuff tears can be asymptomatic and do not always result in loss of function [52]. Yamaguchi et al [16] performed ultrasound on 588 patients who presented with a painful SSP tear and found that 50% of patients above the age of 65 had an asymptomatic SSP tear in their contralateral shoulder. From a biomechanical standpoint, not until a tear

progresses to the critical stage in which it spans the entire SSP tendon will the shoulder's range of motion be mechanically affected [86]. The concept of acute trauma to a chronically torn SSP tendon is a difficult but important issue in the medical field, as treatment methods may differ depending on whether the mechanism of tear was acute or chronic [87] and whether or not there is a high risk of tear propagation during conservative treatment [81, 88-90].

There are several limitations to this portion of the study. Only one specimen was used to confirm similar ultimate load capacity and failure mode in the forward flexed position to previous studies in the abducted position. The two-dimensional calculation of strain for the distal region of the SSP tendon may have slightly underestimated the distal tendon strain due to the out-of-plane wrapping of the tendon around the humeral head. Finally, the strain rate of this specimen is not the same as the strain rate in a rear-end collision. Loads measured at the steering column during low-speed rear-end collisions occurred within approximately 150 ms impulse during the rearward rotation phase and again during the forward rebound phase [27], which would require injury to occur at least 133 times faster than the failure rate of the specimen tested here. However, previous tests have shown that an increase in strain rate does not reduce the ultimate load of a tendon and typically does not affect the failure mode, instead specimen size and clamping technique are more influential on failure mode [91, 92]. In terms of material properties, the tensile strength and strain at failure of the rabbit patella tendon increased by 51 and 77%, respectively, by a 2000-fold increase in strain rate [92].

CONCLUSION

The average orientation of the shoulder blade and arm of drivers holding a steering wheel was quantified. The findings from this study and the literature presented here suggests that tearing of a healthy supraspinatus tendon from a low-speed rear-end automobile collision is unlikely because there is no mechanism or load necessary to sustain an isolated supraspinatus tendon tear. However, tendon degeneration, non-uniform tendon loading, and pre-existing asymptomatic partial or full-thickness tendon tears may alter the risk of a supraspinatus tendon tear or onset of pain in low-speed rear-end collisions.

REFERENCES

1. Adamson GJ, Jackson TJ, McGarry MH, Lee TQ (2015). Biomechanics of the Shoulder: Stability and Kinematics of Shoulder Motion, Throwing Kinematics. *Sports Injuries to the Shoulder and Elbow*, Springer**:** 1-21.

2. Siegmund GP, Chimich DD, Elkin BS (2015). Role of Muscles in Accidental Injury. *Accidental Injury*, Springer**:** 611-642.

3. Oh LS, Wolf BR, Hall MP, Levy BA, Marx RG (2007). Indications for rotator cuff repair: a systematic review. *Clinical orthopaedics and related research,* 455, 52-63.

4. Mather RC, Koenig L, Acevedo D, Dall TM, Gallo P, Romeo A, Tongue J, Williams G (2013). The societal and economic value of rotator cuff repair. *The Journal of Bone & Joint Surgery,* 95(22), 1993-2000.

5. Iannotti JP (1991). *Rotator cuff disorders: evaluation and treatment.* Amer Academy of Orthopaedic.

6. Chakravarty K and Webley M (1993). Shoulder joint movement and its relationship to disability in the elderly. *The Journal of rheumatology,* 20(8), 1359-1361.

7. Matsen F, Arntz C, Lippitt S, Rockwood C (1998). Rotator cuff. *The shoulder,* 2, 755-839.

8. Harryman DT, Hettrich CM, Smith KL, Campbell B, Sidles JA, Matsen FA (2003). A prospective multipractice investigation of patients with full-thickness rotator cuff tears. *J Bone Joint Surg Am,* 85(4), 690-696.

9. Sørensen AK, Bak K, Krarup AL, Thune CH, Nygaard M, Jørgensen U, Sloth C, Torp-Pedersen S (2007). Acute rotator cuff tear: do we miss the early diagnosis? A prospective study showing a high incidence of rotator cuff tears after shoulder trauma. *Journal of Shoulder and Elbow Surgery,* 16(2), 174-180.

10. Mall NA, Lee AS, Chahal J, Sherman SL, Romeo AA, Verma NN, Cole BJ (2013). An evidenced-based examination of the epidemiology and outcomes of traumatic rotator cuff tears. *Arthroscopy: The Journal of Arthroscopic & Related Surgery,* 29(2), 366-376.

11. Aagaard KE, Abu-Zidan F, Lunsjo K (2015). High incidence of acute full-thickness rotator cuff tears: A population-based prospective study in a Swedish Community. *Acta orthopaedica,* 86(5), 558-562.

12. Fukuda H (2003). The management of partial-thickness tears of the rotator cuff. *JOURNAL OF BONE AND JOINT SURGERY-BRITISH VOLUME-,* 85(1), 3-11.

13. Kim HM, Dahiya N, Teefey SA, Middleton WD, Stobbs G, Steger-May K, Yamaguchi K, Keener JD (2010). Location and initiation of degenerative rotator cuff tears. *J Bone Joint Surg Am,* 92(5), 1088-1096.

14. Harris JD, Pedroza A, Jones GL, Baumgarten KM, Bishop JY, Brophy RH, Carey JL, Dunn WR, Holloway GB, Kuhn JE (2012). Predictors of Pain and Function in Patients With Symptomatic, Atraumatic Full-Thickness Rotator Cuff Tears A Time-Zero Analysis of a Prospective Patient Cohort Enrolled in a Structured Physical Therapy Program. *The American Journal of Sports Medicine,* 40(2), 359-366.

15. Sano H, Ishii H, Yeadon A, Backman DS (1997). Degeneration at the insertion weakens the tensile strength of the supraspinatus tendon: a comparative mechanical and histologic study of the bone-tendon complex. *Journal of Orthopaedic Research,* 15(5), 719.

16. Yamaguchi K, Ditsios K, Middleton WD, Hildebolt CF, Galatz LM, Teefey SA (2006). The demographic and morphological features of rotator cuff disease. *J Bone Joint Surg Am,* 88(8), 1699-1704.

17. Milgrom C, Schaffler M, Gilbert S, Van Holsbeeck M (1995). Rotator-cuff changes in asymptomatic adults. The effect of age, hand dominance and gender. *Bone & Joint Journal,* 77(2), 296-298.

18. Sher JS, Uribe JW, Posada A, Murphy BJ, Zlatkin MB (1995). Abnormal findings on magnetic resonance images of asymptomatic shoulders. *J Bone Joint Surg Am,* 77(1), 10-15.

19. Yamamoto A, Takagishi K, Osawa T, Yanagawa T, Nakajima D, Shitara H, Kobayashi T (2010). Prevalence and risk factors of a rotator cuff tear in the general population. *Journal of Shoulder and Elbow Surgery,* 19(1), 116-120.

20. National Highway Traffic Safety Administration (2015). The Economic and Societal Impact of Motor Vehicle Crashes, 2010 (Revised). *Annals of Emergency Medicine,* 66(2), 194-196.

21. Gilroy AM, MacPherson BR, Ross LM (2012). *Atlas of anatomy. 2nd edition*. New York, Thieme.

22. Saccomanno MF, Salvatore M, Grasso A, Milano G (2014). Full-thickness rotator cuff tears. *Shoulder Arthroscopy*, Springer**:** 289-306.

23. National Highway Traffic Safety Administration (2014). Traffic Safety Facts 2014: A Compilation of Motor Vehicle Crash Data from the Fatality Analysis Reporting System and the General Estimates System. (DOT HS 812 261) *US Department of Transportation*.

24. Anderson RD, Welcher JB, Szabo TJ, Eubanks JJ (1998). Effect of braking on human occupant and vehicle kinematics in low speed rear-end collisions. (No. 980298) *SAE Technical Paper*.

25. Braun TA, Jhoun JH, Braun MJ, Wong BM, Boster TA, Kobayashi TM, Perez FA, Hesler GM (2001). Rear-end impact testing with human test subjects. (No. 2001-01-0168) *SAE Technical Paper*.

26. Castro W, Schilgen M, Meyer S, Weber M, Peuker C, Wörtler K (1996). Do" whiplash injuries" occur in low-speed rear impacts? *European spine journal: official publication of the European Spine Society, the European Spinal Deformity Society, and the European Section of the Cervical Spine Research Society,* 6(6), 366-375.

27. Furbish C, Ivory M, Hoffman M, Anderson R, Anderson R (2011). Steering Column Loads and Upper Extremity Motions During Low Speed Rear-End Collisions. (No. 2011-01-0275) *SAE Technical Paper*.

28. Hell W, Langwieder K, Walz F, Muser M, Kramer M, Hartwig E (1999). *Consequences for seat design due to rear end accident analysis, sled tests and possible test criteria for reducing cervical spine injuries after rear-end collision*. Proceedings of the 1999 IRCOBI Conference on the Biomechanics of Impact, Barcelona.

29. Kaneoka K, Ono K, Inami S, Hayashi K (1999). Motion analysis of cervical vertebrae during whiplash loading. *Spine,* 24(8), 763-769.

30. Kumar S, Narayan Y, Amell T (2000). Role of awareness in head-neck acceleration in low velocity rear-end impacts. *Accident Analysis & Prevention,* 32(2), 233-241.

31. Matsushita T, Sato TB, Hirabayashi K, Fujimura S, Asazuma T, Takatori T (1994). X-ray study of the human neck motion due to head inertia loading. (No. 942208) *SAE Technical Paper*.

32. Magnusson M, Pope M, Hasselquist L, Bolte K, Ross M, Goel V, Lee J, Spratt K, Clark C, Wilder D (1999). Cervical electromyographic activity during low-speed rear impact. *European spine journal,* 8(2), 118-125.

33. McConnell WE, Howard RP, Van Poppel J, Krause R, Guzman HM, Bomar JB, Raddin JH, Benedict JV, Hatsell CP (1995). Human head and neck kinematics after low

velocity rear-end impacts-understanding “whiplash”. (No. 952724) *SAE Technical Paper*.

34. Ono K, Kaneoka K, Wittek A, Kajzer J (1997). Cervical injury mechanism based on the analysis of human cervical vertebral motion and head-neck-torso kinematics during low speed rear impacts. (No. 973340) *SAE Technical Paper*.

35. Ono K, Inami S, Kaneoka K, Gotou T, Kisanuki Y, Sakuma S, Miki K (1999). *Relationship between localized spine deformation and cervical vertebral motions for low speed rear impacts using human volunteers*. Proceedings of the International Research Council on the Biomechanics of Injury conference, International Research Council on Biomechanics of Injury.

36. Siegmund GP, King DJ, Lawrence JM, Wheeler JB, Brault JR, Smith TA (1997). Head/neck kinematic response of human subjects in low-speed rear-end collisions. (No. 973341) *SAE Technical Paper*.

37. Siegmund GP, Sanderson DJ, Myers BS, Inglis JT (2003). Awareness affects the response of human subjects exposed to a single whiplash-like perturbation. *Spine,* 28(7), 671-679.

38. Szabo TJ, Welcher JB, Anderson RD, Rice MM, Ward JA, Paulo LR, Carpenter NJ (1994). Human occupant kinematic response to low speed rear-end impacts. (No. 940532) *SAE Technical Paper*.

39. Szabo TJ and Welcher JB (1996). Human subject kinematics and electromyographic activity during low speed rear impacts. (No. 962432) *SAE Technical Paper*.

40. Watanabe Y, Ichikawa H, Kayama O, Ono K, Kaneoka K, Inami S (1999). Relationships Between Occupant Motion and Seat Characteristics in Low-Speed Rear Impacts. (No. 1999-01-0635) *SAE Technical Paper*.

41. Welcher JB, Szabo TJ, Voss DP (2001). Human occupant motion in rear-end impacts: Effects of incremental increases in velocity change. (No. 2001-01-0899) *SAE Technical Paper*.

42. Lucas S, Ianuzzi A, McGowan J, Toosi K (2009). Analysis of Shoulder Ligament Injury Potential in Automotive Rear-End Impacts. (No. 2009-01-1203) *SAE Technical Paper*.

43. Labriola JE, Lee TQ, Debski RE, McMahon PJ (2005). Stability and instability of the glenohumeral joint: the role of shoulder muscles. *Journal of Shoulder and Elbow Surgery,* 14(1), S32-S38.

44. Sporrong H, Palmerud G, Herberts P (1996). Hand grip increases shoulder muscle activity: An EMG analysis with static handcontractions in 9 subjects. *Acta Orthopaedica Scandinavica,* 67(5), 485-490.

45. Wattanaprakornkul D, Halaki M, Cathers I, Ginn KA (2011). Direction-specific recruitment of rotator cuff muscles during bench press and row. *Journal of Electromyography and Kinesiology,* 21(6), 1041-1049.

46. Pappas GP, Blemker SS, Beaulieu CF, McAdams TR, Whalen ST, Gold GE (2006). In vivo anatomy of the Neer and Hawkins sign positions for shoulder impingement. *Journal of Shoulder and Elbow Surgery,* 15(1), 40-49.

47. Valadie AL, Jobe CM, Pink MM, Ekman EF, Jobe FW (2000). Anatomy of provocative tests for impingement syndrome of the shoulder. *Journal of Shoulder and Elbow Surgery,* 9(1), 36-46.

48. McClure PW, Michener LA, Sennett BJ, Karduna AR (2001). Direct 3-dimensional measurement of scapular kinematics during dynamic movements in vivo. *Journal of Shoulder and Elbow Surgery,* 10(3), 269-277.

49. McQuade KJ and Smidt GL (1998). Dynamic scapulohumeral rhythm: the effects of external resistance during elevation of the arm in the scapular plane. *Journal of Orthopaedic & Sports Physical Therapy,* 27(2), 125-133.

50. de Groot JH (1997). The variability of shoulder motions recorded by means of palpation. *Clinical Biomechanics,* 12(7-8), 461-472.

51. Lewis J, Green A, Reichard Z, Wright C (2002). Scapular position: the validity of skin surface palpation. *Manual therapy,* 7(1), 26-30.

52. Keener JD, Hsu JE, Steger-May K, Teefey SA, Chamberlain AM, Yamaguchi K (2015). Patterns of tear progression for asymptomatic degenerative rotator cuff tears. *Journal of Shoulder and Elbow Surgery,* 24(12), 1845-1851.

53. Kijima T, Matsuki K, Ochiai N, Yamaguchi T, Sasaki Y, Hashimoto E, Sasaki Y, Yamazaki H, Kenmoku T, Yamaguchi S (2015). In vivo 3-dimensional analysis of scapular and glenohumeral kinematics: comparison of symptomatic or asymptomatic shoulders with rotator cuff tears and healthy shoulders. *Journal of Shoulder and Elbow Surgery,* 24(11), 1817-1826.

54. McClure PW, Michener LA, Karduna AR, Whitman JM (2006). Shoulder function and 3-dimensional scapular kinematics in people with and without shoulder impingement syndrome. *Physical therapy,* 86(8), 1075.

55. Endo K, Yukata K, Yasui N (2004). Influence of age on scapulo-thoracic orientation. *Clinical Biomechanics,* 19(10), 1009-1013.

56. Manary MA, Reed M, Flannagan CA, Schneider LW (1998). ATD positioning based on driver posture and position. (No. 983163) *SAE Technical Paper*.

57. Lee YS and Lee TQ (2010). Specimen-specific method for quantifying glenohumeral joint kinematics. *Annals of biomedical engineering,* 38(10), 3226-3236.

58. Visible Body (2014). Muscle Premium. Argosy Publishing Inc. Newton, MA. www.visiblebody.com

59. Mihata T, McGarry MH, Ishihara Y, Bui CN, Alavekios D, Neo M, Lee TQ (2015). Biomechanical analysis of articular-sided partial-thickness rotator cuff tear and repair. *The American Journal of Sports Medicine,* 43(2), 439-446.

60. Shin S-J, Yoo JC, McGarry MH, Jun BJ, Lee TQ (2013). Anterior capsulolabral lesions combined with supraspinatus tendon tears: biomechanical effects of the pathologic condition and repair in human cadaveric shoulders. *Arthroscopy: The Journal of Arthroscopic & Related Surgery,* 29(9), 1492-1497.

61. Huffman GR, Tibone JE, McGarry MH, Phipps BM, Lee YS, Lee TQ (2006). Path of glenohumeral articulation throughout the rotational range of motion in a thrower's shoulder model. *The American Journal of Sports Medicine,* 34(10), 1662-1669.

62. Schünke M, Schulte E, Schumacher U, Ross LM, Lamperti ED (2014). *Thieme atlas of anatomy: general anatomy and musculoskeletal system. 2nd edition*. New York, Thieme.

63. Huang H, Zhang J, Sun K, Zhang X, Tian S (2011). Effects of repetitive multiple freeze–thaw cycles on the biomechanical properties of human flexor digitorum superficialis and flexor pollicis longus tendons. *Clinical Biomechanics,* 26(4), 419-423.

64. Bey MJ, Song HK, Wehrli FW, Soslowsky LJ (2002). Intratendinous strain fields of the intact supraspinatus tendon: the effect of glenohumeral joint position and tendon region. *Journal of Orthopaedic Research,* 20(4), 869.

65. van Andel C, van Hutten K, Eversdijk M, Veeger D, Harlaar J (2009). Recording scapular motion using an acromion marker cluster. *Gait & Posture,* 29(1), 123-128.

66. Meskers CG, van de Sande MA, de Groot JH (2007). Comparison between tripod and skin-fixed recording of scapular motion. *Journal of Biomechanics,* 40(4), 941-946.

67. Warner M, Chappell P, Stokes M (2012). Measuring scapular kinematics during arm lowering using the acromion marker cluster. *Human movement science,* 31(2), 386-396.

68. Fayad F, Hoffmann G, Hanneton S, Yazbeck C, Lefevre-Colau M-M, Poiraudeau S, Revel M, Roby-Brami A (2006). 3-D scapular kinematics during arm elevation: effect of motion velocity. *Clinical Biomechanics,* 21(9), 932-941.

69. Lukasiewicz AC, McClure P, Michener L, Pratt N, Sennett B (1999). Comparison of 3-dimensional scapular position and orientation between subjects with and without shoulder impingement. *Journal of Orthopaedic & Sports Physical Therapy,* 29(10), 574-586.

70. Mochizuki T, Sugaya H, Akita K (2009). Humeral insertion of the supraspinatus and infraspinatus. *J Bone Joint Surg Am,* 91(5), 1276-1276.

71. Mihata T, Lee Y, McGarry MH, Abe M, Lee TQ (2004). Excessive humeral external rotation results in increased shoulder laxity. *The American Journal of Sports Medicine,* 32(5), 1278-1285.

72. Kronberg M, Broström L-Å, Söderlund V (1990). Retroversion of the Hurneral Head in the Normal Shoulder and Its Relationship to the Normal Range of Motion. *Clinical orthopaedics and related research,* 253, 113-117.

73. Veeger H, Van Der Helm F, Van Der Woude L, Pronk G, Rozendal R (1991). Inertia and muscle contraction parameters for musculoskeletal modelling of the shoulder mechanism. *Journal of Biomechanics,* 24(7), 615-629.

74. Huang CY, Wang VM, Pawluk RJ, Bucchieri JS, Levine WN, Bigliani LU, Mow VC, Flatow EL (2005). Inhomogeneous mechanical behavior of the human supraspinatus tendon under uniaxial loading. *Journal of Orthopaedic Research,* 23(4), 924-930.

75. Rickert M, Georgousis H, Witzel U (1998). Die native Reißfestigkeit der Sehne des M. supraspinatus beim Menschen. *Der Unfallchirurg,* 101(4), 265-270.

76. Itoi E, Berglund LJ, Grabowski JJ, Schultz FM, Growney ES, Morrey BF, An KN (1995). Tensile properties of the supraspinatus tendon. *Journal of Orthopaedic Research,* 13(4), 578-584.

77. Favre P, Sheikh R, Fucentese SF, Jacob HA (2005). An algorithm for estimation of shoulder muscle forces for clinical use. *Clinical Biomechanics,* 20(8), 822-833.

78. Juul-Kristensen B, Bojsen-Møller F, Holst E, Ekdahl C (2000). Comparison of muscle sizes and moment arms of two rotator cuff muscles measured by ultrasonography and magnetic resonance imaging. *European journal of ultrasound,* 11(3), 161-173.

79. Wood J, Meek SG, Jacobsen S (1989). Quantitation of human shoulder anatomy for prosthetic arm control—I. Surface modelling. *Journal of Biomechanics,* 22(3), 273287-285292.

80. Burkhart SS (2000). A stepwise approach to arthroscopic rotator cuff repair based on biomechanical principles. *Arthroscopy: The Journal of Arthroscopic & Related Surgery,* 16(1), 82-90.

81. Bey MJ, Ramsey ML, Soslowsky LJ (2002). Intratendinous strain fields of the supraspinatus tendon: effect of a surgically created articular-surface rotator cuff tear. *Journal of Shoulder and Elbow Surgery,* 11(6), 562-569.

82. Roh MS, Wang VM, April EW, Pollock RG, Bigliani LU, Flatow EL (2000). Anterior and posterior musculotendinous anatomy of the supraspinatus. *Journal of Shoulder and Elbow Surgery,* 9(5), 436-440.

83. Matsuhashi T, Hooke AW, Zhao KD, Goto A, Sperling JW, Steinmann SP, An KN (2014). Tensile properties of a morphologically split supraspinatus tendon. *Clinical Anatomy,* 27(5), 702-706.

84. Mall N, Kim H, Keener J, Steger-may K, Teefey S, Middleton W, Stobbs G, Yamaguchi K (2011). Symptomatic Progression Of Asymptomatic Rotator Cuff Tears: A Prospective Study Of Clinical And Sonographic Variables. *journal of Orthopaedic & Sports Physical,* 41(5), 368-369.

85. Tashjian RZ (2012). Epidemiology, natural history, and indications for treatment of rotator cuff tears. *Clinics in sports medicine,* 31(4), 589-604.

86. Oh JH, Jun BJ, McGarry MH, Lee TQ (2011). Does a critical rotator cuff tear stage exist? *J Bone Joint Surg Am,* 93(22), 2100-2109.

87. Loew M, Magosch P, Lichtenberg S, Habermeyer P, Porschke F (2015). How to discriminate between acute traumatic and chronic degenerative rotator cuff lesions: an analysis of specific criteria on radiography and magnetic resonance imaging. *Journal of Shoulder and Elbow Surgery,* 24(11), 1685-1693.

88. Miller RM, Fujimaki Y, Araki D, Musahl V, Debski RE (2014). Strain distribution due to propagation of tears in the anterior supraspinatus tendon. *Journal of Orthopaedic Research,* 32(10), 1283-1289.

89. Reilly P, Amis A, Wallace A, Emery R (2003). Mechanical factors in the initiation and propagation of tears of the rotator cuff. *Bone & Joint Journal,* 85(4), 594-599.

90. Reilly P, Amis AA, Wallace AL, Emery RJ (2003). Supraspinatus tears: propagation and strain alteration. *Journal of Shoulder and Elbow Surgery,* 12(2), 134-138.

91. Danto MI and Woo SLY (1993). The mechanical properties of skeletally mature rabbit anterior cruciate ligament and patellar tendon over a range of strain rates. *Journal of Orthopaedic Research,* 11(1), 58-67.

92. Yamamoto N and Hayashi K (1998). Mechanical properties of rabbit patellar tendon at high strain rate. *Bio-medical materials and engineering,* 8(2), 83-90.

APPENDIX A: Driver Motion During a Low-Speed Rear-End Collision

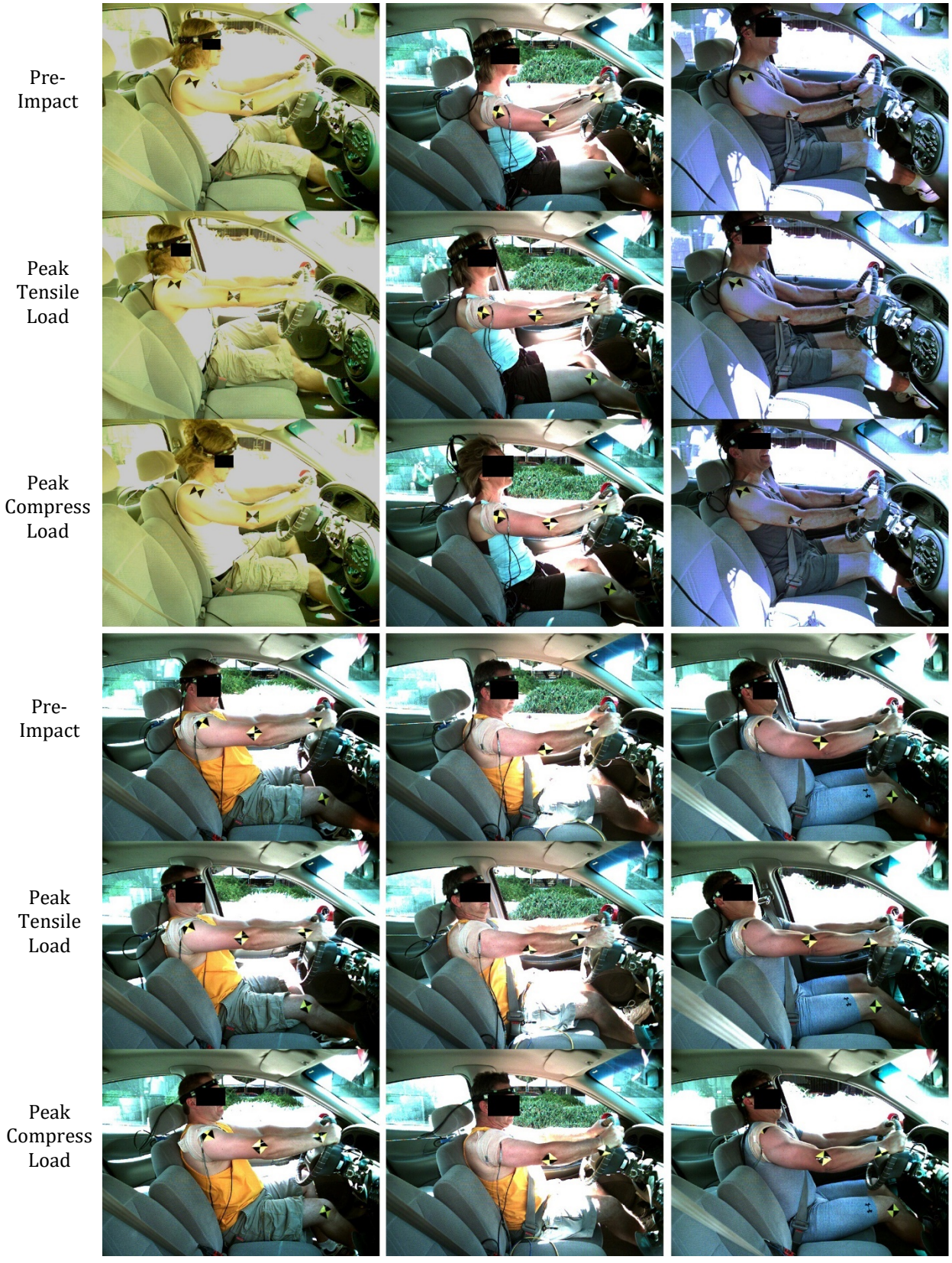

Pre-Impact

Peak Tensile Load

Peak Compress Load

APPENDIX B: Alternative Sequences for Scapula Euler Rotations

Seat Position	Scapula (YX'Z")			Scapula (YZ'X")		
	PT	UR	IR	PT	IR	UR
Reclined	21 ± 7°	8 ± 4°	45 ± 5°	13 ± 7°	45 ± 5°	12 ± 6°
Upright	9 ± 7°	9 ± 4°	42 ± 6°	1 ± 7°	41 ± 6°	12 ± 5°

Seat Position	Scapula (ZX'Y")			Scapula (ZY'X")		
	IR	UR	PT	IR	PT	UR
Reclined	42 ± 6°	21 ± 6°	10 ± 6°	46 ± 5°	9 ± 5°	21 ± 6°
Upright	40 ± 6°	13 ± 6°	1 ± 6°	41 ± 6°	1 ± 6°	13 ± 6°

Seat Position	Scapula (XZ'Y")			Scapula (XY'Z")		
	UR	IR	PT	UR	PT	IR
Reclined	27 ± 6°	39 ± 7°	27 ± 7°	9 ± 5°	21 ± 6°	42 ± 6°
Upright	17 ± 7°	39 ± 6°	12 ± 9°	9 ± 4°	9 ± 7°	40 ± 6°